Universitat Politècnica de Catalunya
Master of Science in Computation Mechanics

Departament de Matemàtica Aplicada III

Relaxation Dynamics of Biological Membranes

by Thiwanka Wickramasooriya

Master's Thesis
Advisor: Marino Arroyo

Barcelona, June 2009

Abstract

Relaxation Dynamics of Biological Membranes

Thiwanka Wickramasooriya

The goal of this project is to explore the relaxation dynamics of lipid fluid membranes which can be found in biological or made-man systems through continuum models and numerical simulations. So far the main focus has been on the equilibrium configurations of vesicles through minimization of the curvature energy subject to constraints. Here, the goal is to describe the time-evolution of out-of-equilibrium vesicle configurations with the effect of the surrounding fluid. This system has two different dissipative mechanisms:

1. membrane dissipation
2. outer flow dissipation

Indeed, bio membranes are 2D fluids due to the large lateral mobility of the components (lipid or other amphiphillic molecules). The membrane dissipation, arising from the friction between the adjacent molecules as they undergo shear is modelled by formulating the Stokes equations on a curved, time evolving surface. The bulk or solution fluid dissipation follows the standard Stokes flow equations. The resulting equations for the coupled system can only be solved analytically in very simple settings. The problem is solved numericaly using a b-spline discretization. The membrane dissipation is solved using b-spline based Galerkin methods and the Stokes dissipation is solved using Boundary Intregal Methods.

Acknowledgments

I would like to express my gratitude to all those who gave me the possibility to complete this thesis. I want to thank the European Commission for giving me the opportunity to study in Europe, University of Swansea, Wales, Universitat Politècnica de Catalunya, Spain and International Center for Numerical Methods in Engineering (CIMNE) for selecting me for this course.

I am deeply indebted to my supervisor Prof. Marino Arroyo from Universitat Politècnica de Catalunya whose help, stimulating suggestions and encouragement helped me in all the time of research for and writing of this thesis.

I would like to thank Prof. Antonio De Simone and Dr. Luca Heltai from Scuola Internazionale Superiore di Studi Avanzati, Trieste, Italy (SISSA) for there help and guidance they gave me. I want to thank everyone at SISSA who helped me on my visit to Italy.

I want to thank all the people who contributed to "GNU Scientific Library (GSL)", and for "A Finite Element Differential Equations Analysis Library(deal.II)".

I want to thank all of my teachers and my colleges from Swansea and Barcelona for all their help, support and valuable hints. Furtermore I want to thank everyone from LaCaN and CIMNE for there help. Especially I am obliged to Ms. Lelia Zelonka for her help in everything.

I would like to thank my former teachers and colleagues at University of Moratuwa, Sri Lanka. I want to thank my parents, my brother and my sister for everything they have done for me.

Contents

List of Figures

List of Tables

List of Boxes

Chapter 1

Introduction

1.1 Motivation

The most notable and the basic difference between a living and a non living system is its ability to sparate itself from its environment so that it can perform some functions which are not possible in its sourrounding environment. This basic form can be seen in all living cells found in single cellular bacteria to most advance creatures like humans. Within the individual cell different vesicles for different functions have to separate themself from each other. For an illustration of a living cell and various vesicles inside see Fig. 1.1.

The basic structure nature invented for this are fluid membranes. In a cell these were made out from lipid bilayer decorated by amphiphilc proteins. Fig. 1.2 These membranes separate each organelle inside the cell from each other as well as individual cell from its surrounding.

Studying the dynamics of the fluid membranes will help to understand the behavior of the cell and its functions. This will help to find more effective drug delivery systems, more effective drugs for diseases and what happens to a cell or organelle when it is sick or in a different environment. Biology is not the only area where fluid membranes were applied. Synthetic biomimitic systems, such as nano-scale chemical reactor networks (Karlsson et al., 2002), are also made out of lipid bilayer fluid membranes. This will also help the possibility of developing bio-mechanical systems such as biosensors.

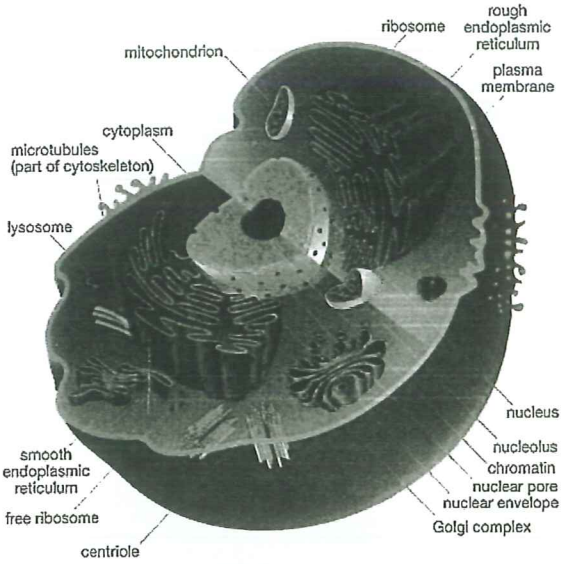

Figure 1.1: Various vesicles inside an animal cell (Port, 2004)

This study is focused on how to use a continuum approach to determine the evolution of fluid membranes. The current methods like Coarse grained Simulation Fig. 1.4 or the Molecular dynamic simulation Fig. 1.3 try to solve this by molecular level approach. These methods have some advantages, They can predict the molecular level processes happening in the membranes, like absorption of foreign partial and can predict physical properties much accurately. If a very detailed analysis is needed these methods are good. The problem with these molecular dynamics simulations is that they can perform very limited size membranes for a very small time period. Just by looking at the pictures one can understand the number of degrees of freedom involved. To solve a whole vesicles membrane up to a comparable time scale with these methods is not possible with the currently available computing power. In most of the situations details up to molecular level is not necessary and only the global behavior of the membrane is needed. In such a situation trying to solve such a large system is a waste of time. This is where the continuum level approach becomes handy, it can predict the overall behavior of the membrane for required time scales. The overall system is million times smaller than the molecular level approach.

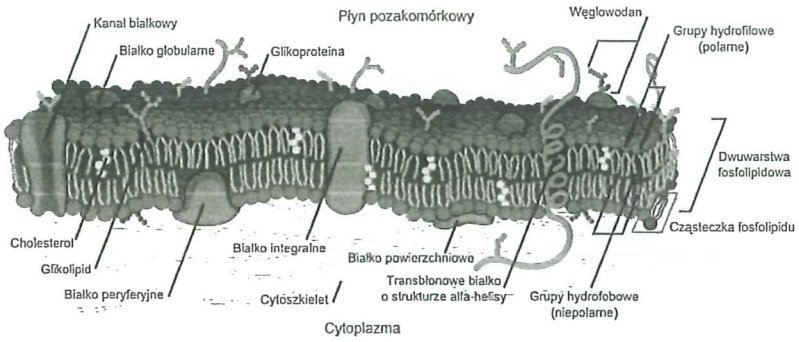

Figure 1.2: Detailed view of lipid bilayer (Ruiz, 2007)

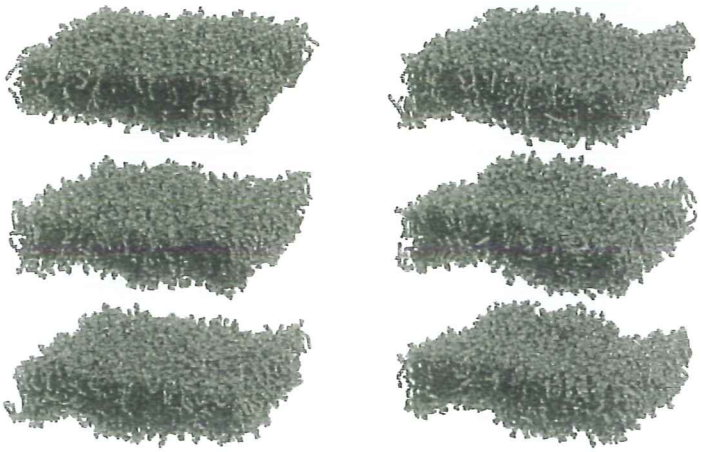

Figure 1.3: Time evolution in a molecular dynamics simulation (E.Lindahl and O.Edholm, 2000)

1.2 Outline

The structure of the presnt report is as follows. The second chapter describes how the mathematical formulation was done. It was given how the physical system was modelled in to mathematical system, the formulation for static case and for dynamic case. Chapter three describes how this mathametical model was discritisize in order to do the numerical simulation. Fourth chapter gives the results from the simulations, describing the qualitative and quantitative difference between each dissipative potential. Chapter five gives conclusions about this study.

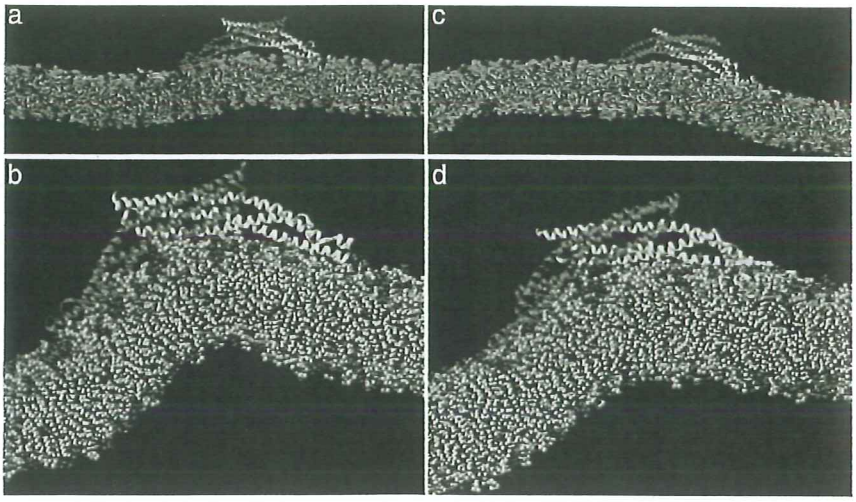

Figure 1.4: Time evolution in a coarse grained simulation (Blood and Voth, 2006)

Chapter 2

Mathematical model

2.1 Curvature elasticity

The equilibrium shape of a fluid membrane is determined by its energy and the imposed constraints. The material parameters of the membrane such as bending rigidity and spontaneous curvature will also play a major role in this. When compared with the size of the vesicle the thickness of the membrane is two or three orders of magnitude smaller. So it can be safely assumed fluid membrane as 2-D surface embedded in 3-D space. It was also assumed that the lipid bilayer is in a fluid state, it will not resist shear forces in the lateral plane.

Any 2D surface Γ can be locally characterized by its two radii of curvature R_1 and R_2. (see Fig. 2.1 for an illustration). The principle curvatures are the reciprocal of them. The surface curvature energy is associated with the mean and the gaussian curvatures which are defined as

$$H = (\frac{1}{R_1} + \frac{1}{R_1}) \qquad\qquad K = (\frac{1}{R_1 R_2})$$

Based on the above assumptions the local energy density can be written as

$$\frac{\kappa}{2}(H - C_0)^2 + \kappa_G K$$

Here the material parameters κ, κ_G are respectively called as bending rigidity and

the gaussian bending rigidity. The bending rigidity of a surface can be evaluated but it is difficult to evaluate the gaussian bending rigidity. C_0 is called as the spontaneous curvature of the surface. This can be considered as a measurement on the asymmetry of the membrane. For instance, the number of lipids can be greater or/and the "head" of the lipids can be larger in one monolayer than in the other. Or the chemical composition of the fluid is different on both sides. C_0 is not supposed to depend on the local shape of the membrane.

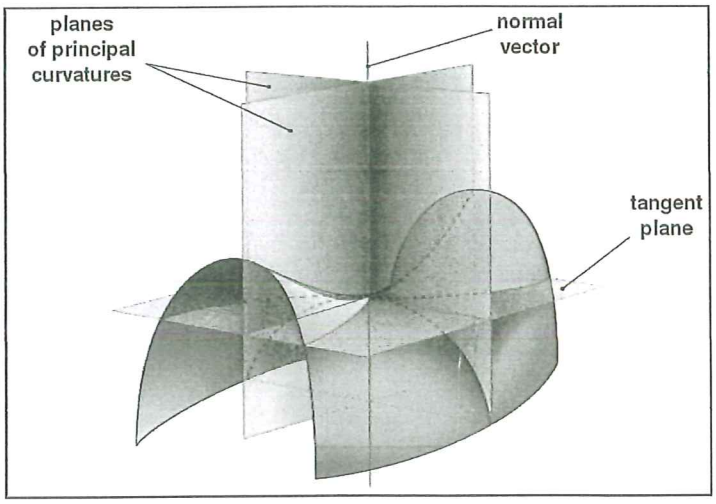

Figure 2.1: Radii of curvature of a surface (Gaba, 2006)

The curvature energy associated with a particular shape is given by integrating the energy density over the surface area. When the above expression is integrated the integral of the gaussian curvature over a closed surface is a topological invariant. The expression for surface energy is (Seifert and Lipowsky, 1995),

$$E_{HC} = \int_{\Gamma} \frac{\kappa}{2}(H - C_0)^2 \, dS$$

The curvature energy E_{HC} is invariant with respect of reparametrizations of the surface, it only depends on the shape. Physically, it does not chage upon tangential velocity fields on the membrane, which do not change the shape. (Arroyo and DeSimone, 2009). In fact it can be shown that other properties such as Volume, Area

are also invariant on parameterization. Even though most of the equations are for a general system our focus will be on the axisymmetric case.

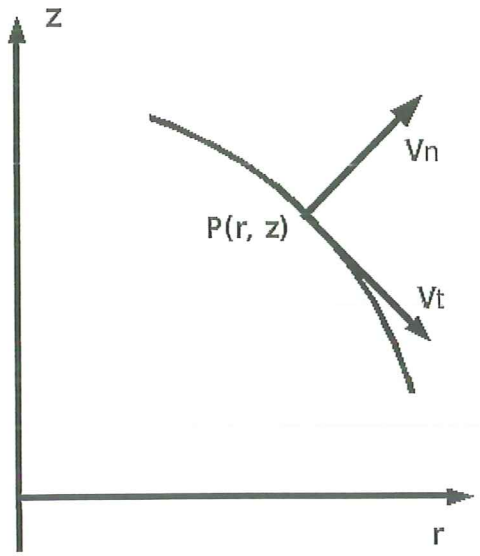

Figure 2.2: Coordinate system used, z-axis is the axis of rotation

We consider cylindrical coordinates, so that the change of variables between cylindrical and cartesian coordinates is geven by

$$\boldsymbol{x}(r, z, \theta) = (r \cos\theta,\ r \sin\theta,\ z)$$

Here the axisymmetric surface is generated by revolving the curve defined in zr plane around z axis. Any point $\boldsymbol{P}(r, z)$ on the generating curve is represented parametrically as $\boldsymbol{P}(r(u), z(u))$, where u is a parameter. Some important parameters of the generating curve can be defined as,

$$a = \sqrt{r'^2 + z'^2}, \qquad b = -r''z' + r'z''$$

The axisymmetric element area is,

$$dS = 2\pi\ ardu$$

A tangent unit vector to the surface in the u direction and a unit normal are

$$\boldsymbol{t} = \frac{1}{a}\{r', z'\}, \quad \boldsymbol{n} = \frac{1}{a}\{-z', r'\}.$$

The velocity of the surface is

$$\boldsymbol{v} = \{\dot{r}, \dot{z}\} = v_t\ \boldsymbol{t} + v_n\ \boldsymbol{n},$$

Where v_t is the tangential velocity field of the membrane and v_n the normal velocity field. hence,

$$v_t = \frac{1}{a}(r'\dot{r} + z'\dot{z}), \quad v_n = \frac{1}{a}(-z'\dot{r} + r'\dot{z}).$$

inversely,

$$\dot{r} = \frac{1}{a}(r'v_t - z'v_n), \quad \dot{z} = \frac{1}{a}(z'v_t + r'v_n)$$

2.2 Dissipative Mechanisms

2.2.1 Mathematical dissipation (L2)

The L_2 or the Willmore flow is a L_2 gradient flow. This is a purely a mathematical model without clear physical interpritation. This is considered because it is a standard measure in the membrane dissipation. The L_2 dissipation is written as

$$W_{L_2}[v_n] = \frac{\hat{\mu}}{2}\int_\Gamma v_n^2\ dS$$

$\hat{\mu}$ is the associated viscosity with the normal direction.

2.2.2 Dissipation in the membrane

The inner flow dissipation is physically meaningful and is the main focus of this study. The surface flow dissipation potentila is derived as (Arroyo and DeSimone, 2009)

$$W_D[v_t, v_n] = \mu \int_\Gamma \left\{ \left(\frac{1}{a} v_t'\right)^2 + \left(\frac{r'}{ar} v_t\right)^2 - \frac{2v_n}{a} \left(\frac{b}{a^3} v_t' + \frac{z'r'}{ar^2} v_t\right) + (H^2 - 2K) v_n^2 \right\} dS$$

This dissipation potential corresponds to a 2D stokes flow on a curved, time evolving surface. This whole study will be based on this equation. The equation given above is derived for the axisymmetric shape. Unlike in L_2 dissipation this equation contains both normal and tangential velocities as well as first derivative of the tangential velocity.

2.2.3 Dissipation in the ambient fluid

This is the dissipation happens due to the viscosity of the sourrounding fluid and it should be included in the total dissipation. If the velocity of the bulk fluid particles adjacent to surface is $\boldsymbol{V}$, Then the rate of deformation tensor can be written as $\boldsymbol{D} = \frac{1}{2}[\nabla \boldsymbol{V} + \nabla \boldsymbol{V}^T]$ and the dissipation ptential in the sourrounding fluid is

$$W_{Dst}[\boldsymbol{V}] = \frac{\mu^b}{2} \int_V \boldsymbol{D} : \boldsymbol{D} \, dV$$

Here dV is the infinitesimal volume element.

2.3 Constraints

The membrane is subjected to three different constraints Area, Volume and the Boundary constraints due to geometrical requirements.

2.3.1 Area Constraint

The membrane is assumed to be inextensible. Because of this the total area of the surface must be remain constant in the dynamics. For the L_2 flow this is applied as a global constraint and for the surface flow this is applied as a local constraint, physically comparable with the surfase Stokes flow. If the total area is,

$$S = \int_\Gamma dS$$

Assuming the surface is closed global area constraint can be defined as

$$0 = \dot{S} = -\int_\Gamma H v_n \, dS.$$

The local area constraint is,

$$0 = -\int_\Gamma p \left[\frac{1}{ar}(r v_t)' - H v_n \right] dS = -\int_\Gamma p \left\{ \frac{1}{ar} \left[\frac{r}{a}(r'\dot{r} + z'\dot{z}) \right]' - \frac{H}{a}(-z'\dot{r} + r'\dot{z}) \right\} dS$$

2.3.2 Volume Constraint

Volume can be either constrained or it can be let free in the dynamics. Physically, the volume constraint is more justified. If the volume is set free the system can evolve until it becomes a sphere in shape. If it is constrained it will evolve to achieve the lowest possible energy with that volume to surface area relation. But for the coupled system with Stokes flow volume must be constrained, because the sourrounding fluid will not allow the membrane to change its volume. It can be proven for the axisymmetric surface the enclosed volume is

$$V = \pi \int r^2 z' \, du$$

Volume constraint,

$$0 = \dot{V} = -\int_\Gamma v_n (2\pi a r) \, du$$

2.3.3 Boundary Conditions

These constraints arise from the geometrical requirements or to prevent translations. So these conditions depend on how the membrane is geometrically defined. For the axisymmetric case geometrical constraints, two to fixe the curve on the axis of rotation, two to keep the end tangencies perpendicular to the symmetric axis. In the case of surface flow dissipation one additional constrain is required to fixed the membrane on z axis, because surface flow do not constrant the translations along the symmetric axis.

2.4 Case studies

2.4.1 Static equilibrium

In the static study we want to find the minimum energy of the membranes under the influence of constant volume and constant area. To find the shape with the minimum curvature energy we start from the simplest shape sphere with a spontaneous curvature C_0 value of zero. Then change the volume and/or spontaneous curvature step by step until the desired values of them are reached.

Mathematical process

In order to get the shape of the minimum energy we find the minimum of the functional which depend on curvature energy (E^{HC}), Volume (V) and the Area (S). But these are not the only thing which going to effect this minimization. We have to take the affect of the parameterization (A) too the energy is invariant w.r.t reparametrization and we need to fix it. We will look for parametrization with approximately constant speed a.

$$A = \int_{\Gamma} (a')^2 dS$$

Using penalty method we can write

$$min\ F = E_{HC} + k_1(V - V_0)^2 + k_2(S - S_0)^2 + k_3 A$$

Here V_0, S_0 are the initial volume and surface area (In this case the volume and area of the starting sphere). k_1, k_2, k_3 are the constant of penalization. This functional is minimized.

Values of k_1, k_2, k_3 are selected by Grosjean (Grosjean, 2008) as 10, 10, 1000. The Augmented Lagrangian formulation was used to remove the parameters k_1, k_2. With this formulation the minimization functional becomes

$$min\ L_A = E_{HC} + k_3 A + \frac{1}{2\beta}\left[(V - V_0)^2 + (S - S_0)^2\right] - \lambda_1(V - V_0) - \lambda_2(S - S_0)$$

β is the penalization parameter and λ are lagrangian multipliers. The Augmented Lagrangian scheme itself takes care of these parameters and the constraints are exactly met within numerical tolerance.

2.4.2 Dynamics

In this section the time evolution of the system is analyzed. This problem is governed by the dissipation and the curvature energy. Without the surrounding fluid the dissipation happens due to membrane dissipation. In the coupled problem (with the sourrounding fluid) dissipation contains membrane dissipation and the Stokes dissipation from the surrounding fluid. Here we study the relaxation of the membrane if suddenly the spontaneous curvature is set to zero and/or if the volume constrain is suddenly removed, so that the membrane is out of equlibrium.

Mathematical process

The behavior of the fluid membrane can be compared with a very simple mechanical system consisting of a spring and a dashpot. Here the dashpot will dissipate energy

in time as a function of velocity. The spring stores the potential energy and absorbs energy propotionally to velocity. This is a conceptual model where the spring stands for the curvature elasticity and the dashpot for the different dissipative mechanisums. The constraints (Area, Volume) are not present in the conceptual model.

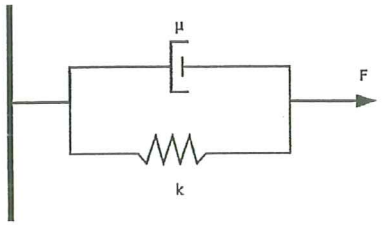

Figure 2.3: Spring Dashpot system

The figure shows a system consisting spring (spring constant k) and a dashpot (viscosity μ) in parallel. The free length of the system is l_0. A constant external force F is applied to the system, the spring is stretched and it will store some energy as potential energy. The system is at equilibrium under the influence of external force F. At an instant this external force is suddenly removed. Now the system is out of equlibrium and tries to achieve a new equlibrium position. Potential energy of the spring at any instant

$$E_k = \frac{1}{2}k(x - l_0)^2$$

Rate of energy release in the spring

$$G_k = -\dot{E}_k = -k(x - l_0)\ \dot{x}$$

The energy dissipation potential in the dashpot is

$$W_D = \frac{1}{2}\mu\dot{x}^2$$

The dynamics of this system are given by the minimum of the difference in energy

release rate in the spring and the energy dissipated in the dashpot :

$$min\ (W_D - G_k)$$

$$min\ (\frac{1}{2}\mu\ \dot{x}^2\ +\ k(x - l_0)\ \dot{x})$$

minimizing this with respect to $\dot{x}$

$$\mu\dot{x} + k(x - l_0) = 0, \quad \text{which is a statement of balance of forces.}$$

By solving this simple differential equation we can get the displacement as a function of time

$$x + l_0 = e^{(-\frac{k}{\mu}t + C)}$$

C is a constant depend on the initial conditions of the system. It can be seen that this system shows an exponential decay. In the dynamics of membrane the same thing happens, the surface is in out of equlibrium state and wants to reduce its extra energy. The dissipation in the membrane and the bulk fluid will act like the dashpot. Here also we are neglecting the inertial effects because for typical membrane, the Reynolds numbers re on the order of 10^{-6} or smaller. We will follow the same procedure to formulate our equations.

One needs to collect all the dissipation potentials into the functional $W[v_t, v_n]$, here quadratic in the velocities. Note that these dissipation contributions can be alternatively written in terms of the rate of change of the parametric curve, i.e. $\tilde{W}[\dot{r}, \dot{z}]$. The energetic mechanisms depend essentially on the shape of the surface, and are collected in $\Pi[\boldsymbol{x}]$. We can compute their rate of change $\dot{\Pi}[\dot{r}, \dot{z}] = \delta_r\Pi \cdot \dot{r} + \delta_z\Pi \cdot \dot{z}$, which depends parametrically on the shape (in the same way that W does) and is linear on the velocities. We typically have (linear) local constraints on the velocities, which we write as $c(v_t, v_n) = 0$ or $\tilde{c}(\dot{r}, \dot{z}) = 0$. We can also have global shape constraints $C[\boldsymbol{x}] = 0$, which we linearize into $\dot{C}[\dot{r}, \dot{z}] = 0$. The dynamics equilibrate the dissipative and the energetic forces, or minimize $W + \dot{\Pi}$ with respect to v_t and v_n or

$\dot{r}$ and $\dot{z}$ subject to the constraints. Forming the Lagrangian

$$\mathcal{L}[\dot{r}, \dot{z}, \lambda](\Lambda) = \tilde{W}[\dot{r}, \dot{z}] + \dot{\Pi}[\dot{r}, \dot{z}] - \int_{\Gamma} \lambda \tilde{c}(\dot{r}, \dot{z}) \, dS - \Lambda \dot{C}[\dot{r}, \dot{z}]$$

we find the velocities at each configuration given by $\boldsymbol{x}$ by finding stationary points, i.e.

$$\delta_{\dot{r}}\mathcal{L} = \delta_{\dot{z}}\mathcal{L} = \delta_{\lambda}\mathcal{L} = \delta_{\Lambda}\mathcal{L} = 0$$

This is the basis for the numerical implimentation.

Chapter 3

Numerical implementation

3.1 Geometry and fields on the membrane

To solve the above equations numerically using a computer, they need to be transformed in to discrete form. There were numeros different schemes to do this. The most famous is to use Galearkin finite element approximation. Normally this method use piecewise C^0 polynomials to approximate the given system and Gauss-Legendre numerical integration to do the required integrations. This type of discritization is not suitable in our case, because the discrete system is only C^0 continuous and the second derivatives do not exists. In the membrane flow equation one needs to compute the second derivatives and curve should be flexible enough to undergo large deformations. In order to over come these difficulties here we use a b-spline base representation of the curve. The curve is now represented parametrically and the actual integration is done not on the curve but on the parametric domain. In otherwords no matter how much the curve is deformed the parametric domain is fixed and invariant in time. And the next nice thing about B-curve is that they are very flexible and one can modify part of the represented curve without affecting the whole curve. The only difficulty with the B-curves is that the calculations are bit more complicated than the standard finite element calculations.

3.1.1 B-splines and their derivatives

In order to define a B-curve two things are needed. The generating control point and associated b-splines. The basis functions or b-splines are defined on the parametric domain u on the knot vector. Knot vector U is the partition of the parametric domain. Each point on the curve is a linear combination of the control points multiplied by the associated values of b-splines. Actually each section on the knot vector will generate one part of the curve called as a Bazier curve. The final curve is a combination of all the Bazier curves Fig. 3.1. The degree of the generated curve is depend on the degree of associate b-splines. Polygon made by the control points is called as the control polygon. The resulting curve full fill the property called convex hull, the generated curve is always inside the control polygon. If u is a parameter then any point $\boldsymbol{C}$ on the curve is given by

$$C(u) = \sum_{i=1}^{n+1} N_{i,p}(u)\boldsymbol{P_i}, \quad \text{so} \qquad \begin{aligned} r(u) &= \textstyle\sum_{i=1}^{n+1} N_{i,p}(u) r_i \\ z(u) &= \textstyle\sum_{i=1}^{n+1} N_{i,p}(u) r_i \end{aligned}$$

Here $\boldsymbol{P_i}$ is ith the control point and $N_{i,p}(u)$ is the ith basis function. p represent the degree of the basis functions.

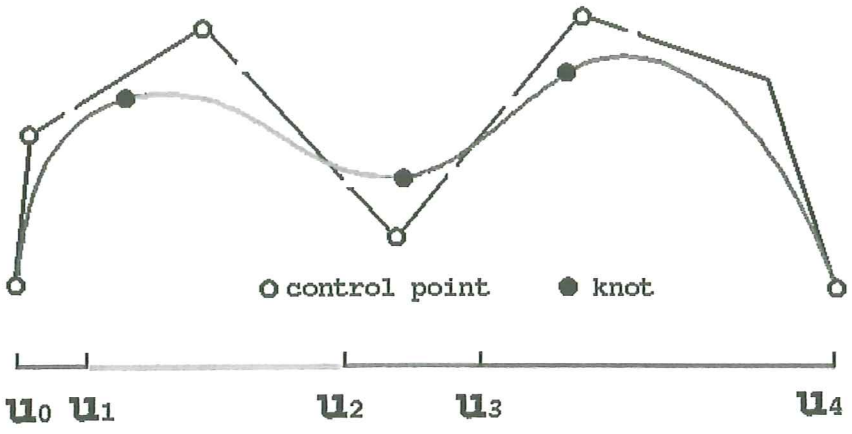

Figure 3.1: Individual Bazier parts and respective knots (Laboratory, 2004)

The knot vector U is defined as

$$U = \left\{ \overbrace{\underbrace{0, 0....0}_{p+1}, u_{p+1}, u_{p+2}.....u_{m-p-1}, \underbrace{1, 1....1}_{p+1}}^{m+1} \right\}$$

Here $n+1$ is the number of control points and $m+1$ is the number of knots in U vector.

In general U do not need to be defined between 0 and 1. The knots can be placed as one wish them to be, even you can have repeated knots just like in the start and at end. But for our study in order to keep things consistant and to make the integration easy the knot vector is strictly defined between 0 and 1, the knots are equally spaced and don't have any repeating knots except for start and end (non periodic and uniform).

For a non periodic and uniform knot vector n, p, m related as

$$n = m - p - 1$$

The basis functions (b-splines) are defined on this knot vector as, (Peegl and Tiller, 1997)

$$N_{i,0}(u) = \begin{cases} 1 & \text{if } u_i < u \leq u_{i+1} \\ 0 & \text{otherwise} \end{cases}$$

$$N_{i,p}(u) = \frac{u - u_i}{u_{i+p} - u_i} N_{i,p-1}(u) + \frac{u_{i+p+1} - u}{u_{i+p+1} - u_{i+1}} N_{i+1,p-1}(u)$$

It was defined that $\frac{0}{0} = 0$

First derivative of the curve $\boldsymbol{C}$ can be calculated as (Peegl and Tiller, 1997)

$$\boldsymbol{C}(u)' = \sum_{i=1}^{n+1} N_{i,p}(u)' \boldsymbol{P_i}$$

where

$$N_{i,p}(u)' = \frac{p}{u_{i+p} - u_i} N_{i,p-1}(u) + \frac{p}{u_{i+p+1} - u_{i+1}} N_{i+1,p-1}(u)$$

Higher order derivatives are computed by applying this recursively. In the implementation however modified algorithms are used to calculate the b-splines and there

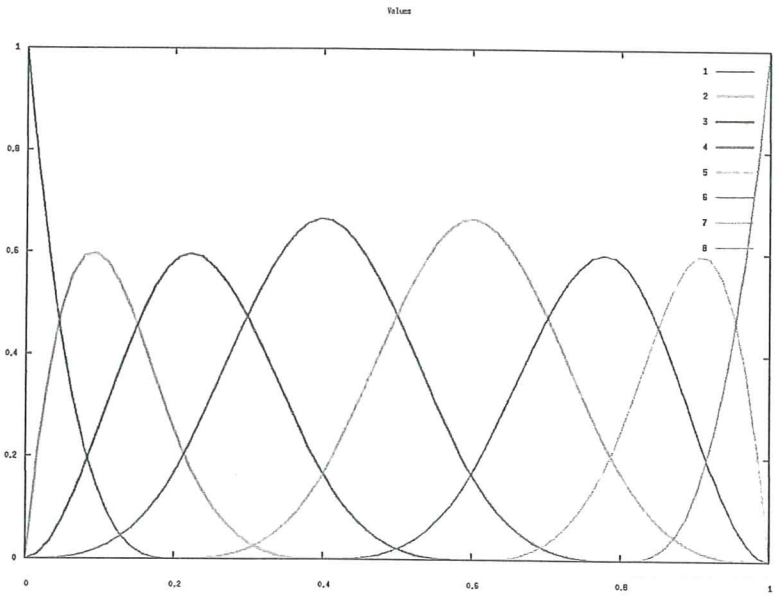

Figure 3.2: Cubic b-Spline functions

derivatives more efficiently. With each load step or with each time step we are going to modify the position of the control points. It is required to calculate all the gradients and the damping matrices with respect to control points.

3.1.2 Static analysis

For the static analysis the minimization is done using the matlab fmincon function and we need to supply the gradient of the minimization functional with respect to each control points.

$$\nabla L_A = \left(\frac{\partial L_A}{\partial \boldsymbol{r_I}}, \frac{\partial L_A}{\partial \boldsymbol{z_I}} \right)$$

Here $(\boldsymbol{r_I}, \boldsymbol{z_I})$ represent the control points.

$$\frac{\partial L_A}{\partial \boldsymbol{r_I}} = \frac{\partial E_{HC}}{\partial \boldsymbol{r_I}} + k_3 \frac{\partial A}{\partial \boldsymbol{r_I}} + \frac{1}{\beta} \left[(V - V_0) \frac{\partial V}{\partial \boldsymbol{r_I}} + (S - S_0) \frac{\partial S}{\partial \boldsymbol{r_I}} \right] - \lambda_1 \frac{\partial V}{\partial \boldsymbol{r_I}} - \lambda_2 \frac{\partial S}{\partial \boldsymbol{r_I}}$$

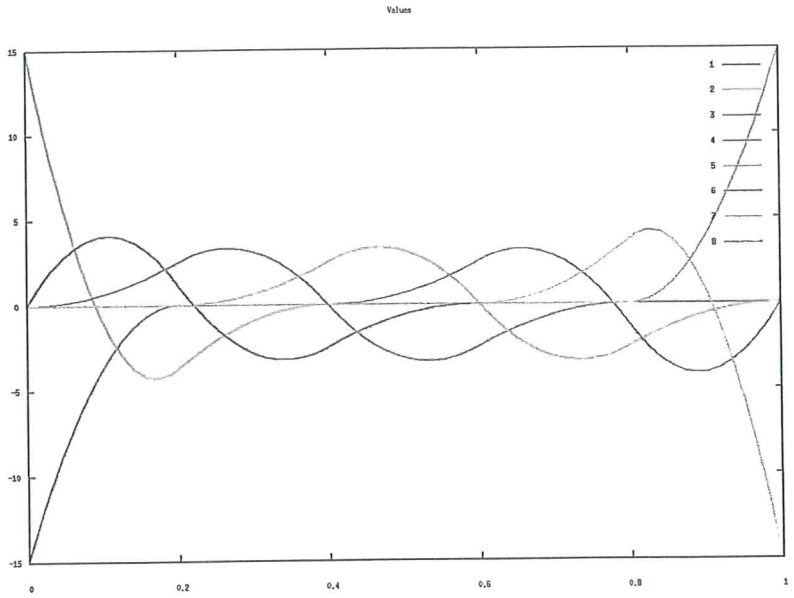

Figure 3.3: Cubic b-Spline function's first derivatives

$$\frac{\partial L_A}{\partial z_I} = \frac{\partial E_{HC}}{\partial z_I} + k_3 \frac{\partial A}{\partial z_I} + \frac{1}{\beta}\left[(V - V_0)\frac{\partial V}{\partial z_I} + (S - S_0)\frac{\partial S}{\partial z_I}\right] - \lambda_1 \frac{\partial V}{\partial z_I} - \lambda_2 \frac{\partial S}{\partial z_I}$$

$$\begin{array}{ll}
\frac{\partial r}{\partial r_I} = N_I & \frac{\partial r}{\partial z_I} = 0 \\
\frac{\partial z}{\partial r_I} = 0 & \frac{\partial z}{\partial z_I} = N_I' \\
\frac{\partial a}{\partial r_I} = \frac{r'}{a} N_I & \frac{\partial z}{\partial z_I} = \frac{z'}{a} N_I' \\
\frac{\partial b}{\partial r_I} = -z' N_I'' + z'' N_I' & \frac{\partial z}{\partial z_I} = -r' N_I'' + r'' N_I' \\
\frac{\partial H^2}{\partial r_I} = 2H \frac{\partial H}{\partial r_I} & \frac{\partial H^2}{\partial z_I} = 2H \frac{\partial H}{\partial z_I} \\
\frac{\partial (a')^2}{\partial r_I} = \frac{2a'}{a}\left[N_I' r'' + r' N_I'' - a' \frac{\partial a}{\partial r_I}\right] & \frac{\partial (a')^2}{\partial z_I} = \frac{2a'}{a}\left[N_I' z'' + z' N_I'' - a' \frac{\partial a}{\partial z_I}\right] \\
\frac{\partial H}{\partial r_I} = \frac{1}{a^3}\frac{\partial b}{\partial r_I} + \left[\frac{3b}{a^4} + \frac{z'}{ra^2}\right]\frac{\partial a}{\partial r_I} - \frac{z' N_I}{r^2 a} & \frac{\partial H}{\partial z_I} = \frac{1}{a^3}\frac{\partial b}{\partial z_I} + \left[\frac{3b}{a^4} + \frac{z'}{ra^2}\right]\frac{\partial a}{\partial z_I} - \frac{N_I'}{ra}
\end{array}$$

Box 3.1: Basic derivatives w.r.t Control Points (Grosjean, 2008)

Using the basic derivations given above we can compute the derivatives of Energy, Volume, Area and parameterization functional(A).

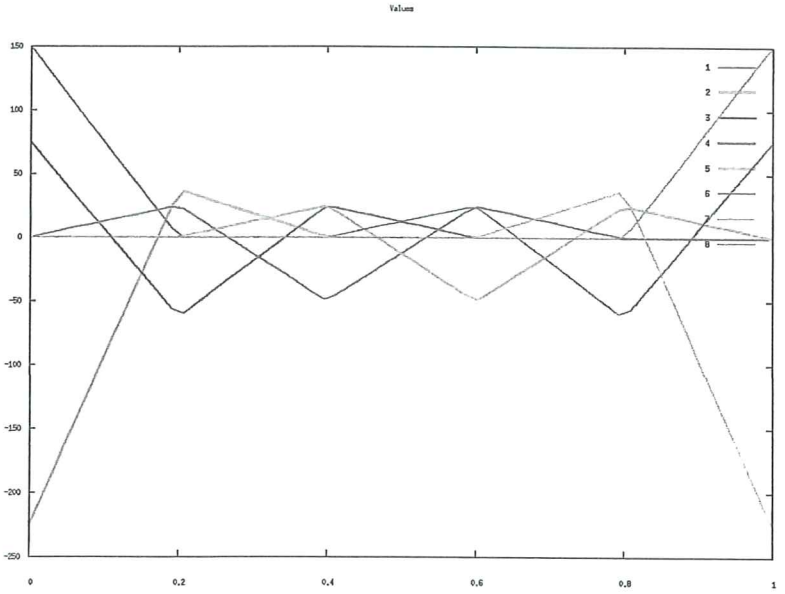

Figure 3.4: Cubic b-Spline function's second derivatives

Energy (E^{HC})

$$\frac{\partial E^{HC}}{\partial \boldsymbol{r_I}} = 2\pi \int \frac{\kappa}{2} \left[2(H - C_0) a r \frac{\partial H}{\partial \boldsymbol{r_I}} + (H - C_0)^2 \left(r \frac{\partial a}{\partial \boldsymbol{r_I}} + a N_I \right) \right] du$$

$$\frac{\partial E^{HC}}{\partial \boldsymbol{z_I}} = 2\pi \int \frac{\kappa}{2} \left[2(H - C_0) a r \frac{\partial H}{\partial \boldsymbol{z_I}} + (H - C_0)^2 r \frac{\partial a}{\partial \boldsymbol{z_I}} \right] du$$

Volume (V)

$$\frac{\partial V}{\partial \boldsymbol{r_I}} = 2\pi \int z' r N_I du \qquad \frac{\partial V}{\partial \boldsymbol{z_I}} = 2\pi \int \frac{r^2}{2} N_I du$$

Area (S)

$$\frac{\partial S}{\partial \boldsymbol{r_I}} = 2\pi \int \left(r \frac{\partial a}{\partial \boldsymbol{r_I}} + a N_I \right) du \qquad \frac{\partial S}{\partial \boldsymbol{z_I}} = 2\pi \int r \frac{\partial a}{\partial \boldsymbol{z_I}} du$$

Parameterization (A)

$$\frac{\partial A}{\partial \boldsymbol{r_I}} = 2\pi \int \left[(a')^2 \left(r \frac{\partial a}{\partial \boldsymbol{r_I}} + a N_I \right) + \frac{\partial (a')^2}{\partial \boldsymbol{r_I}} ar \right] du$$

$$\frac{\partial A}{\partial \boldsymbol{z_I}} = 2\pi \int \left[(a')^2 r \frac{\partial a}{\partial \boldsymbol{z_I}} + \frac{\partial (a')^2}{\partial \boldsymbol{z_I}} ar \right] du$$

The gradient of the minimization functional is calculated using above values.

3.1.3 Dynamics analysis

Similarly to the spring dashpot system, after discretization, we obtain a system of ODE, which includes the componants,

$$\begin{aligned} \boldsymbol{D(P)\dot{P} + L(P)\lambda} &= \boldsymbol{f}_{elastic}(\boldsymbol{P}) \\ \boldsymbol{L(P)}^T \boldsymbol{\dot{P}} &= \boldsymbol{0} \end{aligned}$$

we next derive the expressions for the matrices and forcing vectors above.

Energetic contributions: curvature elasticity

We consider the curvature energy. In the static analysis of membranes, one computes

$$f_{Ir}^{HC} = \delta_r G_{HC} \cdot N_I = -\frac{\partial E_{HC}}{\partial r_I}$$

and

$$f_{Iz}^{HC} = \delta_z G_{HC} \cdot N_I = -\frac{\partial E_{HC}}{\partial z_I}.$$

These are the contributions to $\boldsymbol{f}_{elastic}(\boldsymbol{P})$ from curvature elasticity.

Dissipative contributions

For the ease of calculations for a point u, which lies in side the i th knot span one can define, The local velocities,

$$\boldsymbol{v}_n^{crve}(u) = [-z' \quad r'] \qquad\qquad \boldsymbol{v}_t^{crve}(u) = [r' \quad z']$$

The local b-spline matrix,

$$\boldsymbol{N}^{loc}(u) = \begin{bmatrix} N_{i-(p-2)} & 0 \\ 0 & N_{i-(p-2)} \\ N_{i-(p-1)} & 0 \\ 0 & N_{i-(p-1)} \\ \vdots & \vdots \\ N_{i+p-1} & 0 \\ 0 & N_{i+p-1} \end{bmatrix}$$

The corrosponding global connectivity matrix,

$$T = \begin{bmatrix} a_1^r, a_1^r & a_1^r, a_1^z & a_1^r, a_2^r & a_1^r, a_2^z & \cdots & a_1^r, a_m^r & a_1^r, a_m^z \\ a_1^z, a_1^r & a_1^z, a_1^z & a_1^z, a_2^r & a_1^z, a_2^z & \cdots & a_1^z, a_m^r & a_1^z, a_m^z \\ a_2^r, a_1^r & a_2^r, a_1^z & a_2^r, a_2^r & a_2^r, a_2^z & \cdots & a_2^r, a_m^r & a_2^r, a_m^z \\ a_2^z, a_1^r & a_2^z, a_1^z & a_2^z, a_2^r & a_2^z, a_2^z & \cdots & a_2^z, a_m^r & a_2^z, a_m^z \\ \vdots & \vdots & \vdots & \vdots & \ddots & \vdots & \\ a_n^r, a_1^r & a_n^r, a_2^z & a_n^r, a_2^r & a_n^r, a_2^z & \cdots & a_n^r, a_m^r & a_n^r, a_m^z \\ a_n^z, a_1^r & a_n^z, a_2^z & a_n^z, a_2^r & a_n^z, a_2^z & \cdots & a_n^z, a_m^r & a_n^r, a_m^z \end{bmatrix}$$

where

$$\begin{aligned} a_m^r &= 2\,(i+k) \\ a_n^r &= 2\,(i+k) \\ a_m^z &= 2\,(i+k)) + 1 \\ a_n^z &= 2\,(i+k) + 1 \end{aligned}$$

$$k = -(p-2), -(p-1), ..., (p-1)$$

L_2 dissipation

The L_2 dissipation is

$$W_{L_2}[v_n] = \frac{\hat{\mu}}{2}\int_\Gamma v_n^2 dS, \qquad \tilde{W}_{L_2}[\dot{r}, \dot{z}] = \frac{\hat{\mu}}{2}\int_\Gamma \frac{1}{a^2}(-z'\dot{r} + r'\dot{z})^2 dS.$$

Its variation follows as

$$\delta\tilde{W}_{L_2} = \hat{\mu}\int_\Gamma \frac{1}{a^2}(-z'\dot{r} + r'\dot{z})(-z'\delta\dot{r} + r'\delta\dot{z})\ dS$$

If we define a local matrix $\boldsymbol{B}_n$ as,

$$\boldsymbol{B}_n = \frac{1}{a}\boldsymbol{v}_n^{crve}\boldsymbol{N}^{loc}$$

which gives the local damping matrix,

$$D_{n,loc}^{L_2} = \hat{\mu}\int_\Gamma \boldsymbol{B}_n\boldsymbol{B}_n^T 2\pi a r du$$

This local $D_{n,loc}^{L_2}$ damping matrix is assembled to the correct positions in the damping matrix $D^{L_2,n}$ using the connectivity matrix T.
Note that the field v_t remains largely undetermined with only this dissipation source. To eliminate the indeterminacy we introduce the artificial dissipation

$$W_{L_2,t}[v_t] = \frac{\tilde{\mu}}{2}\int_\Gamma v_t^2 dS.$$

like in the previous case we can calculate $\boldsymbol{B}_t$ as,

$$\boldsymbol{B}_t = \frac{1}{a}\boldsymbol{v}_t^{crve}\boldsymbol{N}^{loc}$$

which gives the local damping matrix,

$$D_{t,loc}^{L_2} = \tilde{\mu}\int_\Gamma \boldsymbol{B}_t\boldsymbol{B}_t^T 2\pi a r du$$

This is assembled to $D^{L_2,t}$ get the final tangential damping matrix. The results should be insensitive to the choice of $\tilde{\mu}$, so a good choice for matrix conditioning is simply $\tilde{\mu} = \hat{\mu}$.

Surface flow dissipation

The physical inner flow dissipation reads

$$W_D[v_t, v_n] = \mu \int_\Gamma \left\{ \left(\frac{1}{a} v_t'\right)^2 + \left(\frac{r'}{ar} v_t\right)^2 - \frac{2v_n}{a}\left(\frac{b}{a^3} v_t' + \frac{z'r'}{ar^2} v_t\right) + (H^2 - 2K) v_n^2 \right\} dS$$

or

$$\begin{aligned} W_D[\dot{r}, \dot{z}] = \mu \int_\Gamma \Bigg\{ & \frac{1}{a^2}\left[\left(\frac{r'\dot{r} + z'\dot{z}}{a}\right)'\right]^2 + \left[\frac{r'}{a^2 r^2}\left(\frac{r'\dot{r} + z'\dot{z}}{a}\right)\right]^2 \\ & - \frac{2}{a}\left(\frac{-z'\dot{r} + r'\dot{z}}{a}\right)\left[\frac{b}{a^3}\left(\frac{r'\dot{r} + z'\dot{z}}{a}\right)' + \frac{z'r'}{ar^2}\left(\frac{r'\dot{r} + z'\dot{z}}{a}\right)\right] \\ & + (H^2 - 2K)\left(\frac{-z'\dot{r} + r'\dot{z}}{a}\right)^2 \Bigg\} \; dS \end{aligned}$$

Its variation is

$$\begin{aligned} W_D[\dot{r}, \dot{z}, \delta\dot{r}, \delta\dot{z}] = \mu \int_\Gamma \Bigg\{ & \frac{2}{a^2}\left[\frac{r'\dot{r} + z'\dot{z}}{a}\right]'\left[\frac{r'\delta\dot{r} + z'\delta\dot{z}}{a}\right]' + \frac{2r'}{a^2 r^2}\left(r'\dot{r} + z'\dot{z}\right)\left(r'\delta\dot{r} + z'\delta\dot{z}\right) \\ & - \frac{2b}{a^5}\left[\left(-z'\dot{r} + r'\dot{z}\right)\left(\frac{r'\delta\dot{r} + z'\delta\dot{z}}{a}\right)' + \left(-z'\delta\dot{r} + r'\delta\dot{z}\right)\left(\frac{r'\dot{r} + z'\dot{z}}{a}\right)'\right] \\ & - \frac{2z'r'}{a^4 r^2}\left[\left(-z'\dot{r} + r'\dot{z}\right)\left(r'\delta\dot{r} + z'\delta\dot{z}\right) + \left(-z'\delta\dot{r} + r'\delta\dot{z}\right)\left(r'\dot{r} + z'\dot{z}\right)\right] \\ & + 2\left(\frac{H^2 - 2K}{a^2}\right)\left(-z'\dot{r} + r'\dot{z}\right)\left(r'\delta\dot{r} + z'\delta\dot{z}\right) \Bigg\} \; dS \end{aligned}$$

If the derivative of $\boldsymbol{v}_t^{loc}$ w.r.t u is

$$(\boldsymbol{v}')_t^{crve}(u) = [r'' \quad z'']$$

We can calculate the $\boldsymbol{B}'_t$ by differentiating the $\boldsymbol{B}_t$ matrix w.r.t u as,

$$\boldsymbol{B}'_t = (\boldsymbol{v}')_t^{crve} \boldsymbol{N}^{loc} + \boldsymbol{v}_t^{crve} (\boldsymbol{N}')^{loc}$$

Now the resulting local damping matrix for membrane dissipation can be calculated as

$$D_{loc}^{mem} = 2\mu \int_\Gamma \left\{ \frac{1}{a^2} \boldsymbol{B'}_t \boldsymbol{B'}_t^T + \frac{(r')^2}{a^2 r^2} \boldsymbol{B}_t \boldsymbol{B}_t^T - \frac{\boldsymbol{B}_n}{a} \left(\frac{b}{a^3} \boldsymbol{B'}_t^T + \frac{z'r'}{ar^2} \boldsymbol{B}_t^T \right) \right.$$
$$\left. - \frac{\boldsymbol{B'}_n^T}{a} \left(\frac{b}{a^3} \boldsymbol{B'}_t + \frac{z'r'}{ar^2} \boldsymbol{B}_t \right) + (H^2 - 2K) \boldsymbol{B}_n \boldsymbol{B}_n^T \right\} \, dS$$

Like in the L_2 damping matrix we need to assemble thease local matrices in to the resulting membrane dissipation damping matrix D^{mem} using the connectivity matrix T.

Constraints

Volume constraint

Assuming the surface has no free end, this single constraint is simply

$$0 = \dot{V} = -\int_\Gamma v_n (2\pi a r) \, du$$

The resulting constraint vector is

$$L_{Ir}^{vol} = \int_\Gamma N_I z' 2\pi r \, du \qquad L_{Iz}^{vol} = -\int_\Gamma N_I r' 2\pi r \, du.$$

Global area constraint

This single constraint is simply

$$0 = \dot{S} = -\int_\Gamma H v_n \, dS \pm 2\pi r v_t \big|_{boundary}.$$

Assuming the surface is closed, the resulting constraint vector is

$$L_{Ir}^{surf} = \int_\Gamma N_I H z' 2\pi r \, du \qquad L_{Iz}^{surf} = -\int_\Gamma N_I H r' 2\pi r \, du.$$

Local area constraints

The weak statement of the constraint is

$$\begin{aligned} 0 &= -\int_\Gamma p\left[\frac{1}{ar}(rv_t)' - Hv_n\right] dS = -\int_\Gamma p\left\{\frac{1}{ar}\left[\frac{r}{a}(r'\dot{r}+z'\dot{z})\right]' - \frac{H}{a}(-z'\dot{r}+r'\dot{z})\right\} dS \\ &= -\int_\Gamma p\Bigg\{\underbrace{\left[r'\frac{r'a-ra'}{ra^2}+\frac{r''}{a}+Hz'\right]}_{A}\dot{r} + \underbrace{\left[z'\frac{r'a-ra'}{ra^2}+\frac{z''}{a}-Hr'\right]}_{B}\dot{z} + \frac{r'}{a}\dot{r}' + \frac{z'}{a}\dot{z}'\Bigg\} 2\pi r\, du \end{aligned}$$

which results in the constraint matrices

$$L^p_{IJr} = -\int_\Gamma \hat{N}_I\left(AN_J + \frac{r'}{a}N'_J\right) 2\pi r\, du, \qquad L^p_{IJz} = -\int_\Gamma \hat{N}_I\left(BN_J + \frac{z'}{a}N'_J\right) 2\pi r\, du.$$

Boundary conditions

For a symmetry boundary point, one has for each configuration that $r = 0$ and $z' = 0$. The time-evolution needs to preserve these conditions, hence

$$\dot{r} = \dot{z}' = 0, \quad \text{or,} \quad \dot{r}_1 = \dot{r}_n = 0, \dot{z}_1 - \dot{z}_2 = \dot{z}_{n-1} - \dot{z}_n = 0,$$

resulting in the matrix

$$\boldsymbol{L}^{BC} = \begin{bmatrix} 1 & 0 & 0 & 0 & \cdots & 0 & 0 & 0 & 0 \\ 0 & 0 & 0 & 0 & \cdots & 0 & 0 & 1 & 0 \\ 0 & 1 & 0 & -1 & \cdots & 0 & 0 & 0 & 0 \\ 0 & 0 & 0 & 0 & \cdots & 0 & 1 & 0 & -1 \end{bmatrix}^T$$

When the membrane dissipaion is consider without Stokes dissipation another additional boundary condition needs to be included to prevent the translation along z

axis. now,

$$\boldsymbol{L}_{mem}^{BC} = \begin{bmatrix} 1 & 0 & 0 & 0 & \cdots & 0 & \cdots & 0 & 0 & 0 & 0 \\ 0 & 0 & 0 & 0 & \cdots & 0 & \cdots & 0 & 0 & 1 & 0 \\ 0 & 0 & 0 & 0 & \cdots & z_{mid} & \cdots & 0 & 0 & 0 & 0 \\ 0 & 1 & 0 & -1 & \cdots & 0 & \cdots & 0 & 0 & 0 & 0 \\ 0 & 0 & 0 & 0 & \cdots & 0 & \cdots & 0 & 1 & 0 & -1 \end{bmatrix}^T$$

Numerical Integration

All the integrals are evaluated using Gauss Legendra quadrature rules. The order of the quadrature rule should be change according to the degree of the b-splines. If not under integration can happen and the values obtained will be not correct. Here the integration is performed on the u space. The integration are the knot spans, because at each knot the piecewice polynominal definition of the b-spline are changing Fig. 3.5. If the function being integrated is $f(u)$ we can write,

$$\int_{u=0}^{u=1} f(u)dS = 2\pi \sum_{i=1}^{i=m-2p} \int_{u=u_i}^{u=u_{i+1}} f(u)ardu$$

then applying the numerical integration

$$2\pi \sum_{i=1}^{i=m-2p} \int_{u=u_i}^{u=u_{i+1}} f(u)ardu = 2\pi \sum_{i=1}^{i=m-2p} \left(\frac{u_{i+1}-u_i}{2} \sum_{j=1}^{N_g} w_j f(u_{ij})a(u_{ij})r(u_{ij}) \right)$$

where u_{ij} is the jth Gauss point of the ith interval considered and N_g the number of Gauss points considered in each subintervals. w_j is the gauss weight associated with each jth gauss point.

Figure 3.5: Gauss points inside each knot span.

3.2 Boundary Element Method (BEM)

To couple the effect of the surrounding fluid the boundary integral methods are used. In the relaxation of fluid membranes the main focus is to study the behavior of the membrane, so we only need to get the effect of sourrounding fluid as the membrane evolve in time. In this analysis the vesicle is assumed to be surrounded by an infinitely large fluid domain. Here the system will not be solved for the surrounding fluid domain, but only the effect of the bulk fluid on the membrane is calculated. It is possible to calculate the behavior of the sourrounding fluid but it is not in our interest. The governing force of the relaxation of the membrane is the curvature energy. Ignoring constraints for the sake of simplicity, it was calculated as

$$f^{HC} = D\dot{\boldsymbol{P}}$$

D is the damping matrix of the system.

The goal is now to obtain the effective damping matrix acting on the control points describing the surface, encoding the effect of the sourrounding fluid. If σ is the traction and v is the membrane velocity then,

$$Power = \int_{\Gamma} \sigma v \; dS$$

Using b-spline basis functions we can approximate v as $\Sigma_i N_i \dot{\boldsymbol{P}}_i$ It is not necessary to use the same basis functions (same elements) for membrane dissipation and for BEM. Finally the two systems should be coupled in order to solve. The relationship between these systems can be developed as

$$\begin{aligned} Power &= \int_{\Gamma} \sigma \; \Sigma_i N_i \dot{\boldsymbol{P}}_i \; dS \\ &= \Sigma_i \int_{\Gamma} \sigma N_i dS \; \dot{\boldsymbol{P}}_i = \Sigma_i f_i dS \; \dot{\boldsymbol{P}}_i \end{aligned}$$

Using different set of basis functions (φ_k) traction can be represented as

$$\sigma = \Sigma_k \; F_k \varphi_k$$

again Power can be written as

$$\begin{aligned} Power &= \int_\Gamma \sigma v \; dS \\ &= \int_\Gamma \Sigma_k F_k \varphi_k \; u dS \\ &= \Sigma_k \; F_k \int_\Gamma \varphi_k u dS \\ &= \Sigma_k \; F_k \int_\Gamma \varphi_k \Sigma_i N_i dS \dot{\boldsymbol{P}}_i \\ &= \Sigma_k \Sigma_i \int_\Gamma \varphi_k N_i \; F_k dS \dot{\boldsymbol{P}}_i \end{aligned}$$

From the above equations

$$f_i = \int_\Gamma \varphi_k N_i dS \; F_k = M_{ik} F_k$$

$$f = MF$$

where $M_{ik} = \int_\Gamma \varphi_k N_i dS$. This is the matrix coupling the two different finite elements used in the coupled problem.

BEM Formulation

Using single layer potential the velocity can be calculated as

$$v = -\frac{1}{8\pi\mu_b} \int_\Gamma G\sigma dS$$

G is the single layer stokeslet for the boundary elements and the μ_b is the viscosity of the surrounding fluid. For free space this is defined as (Pozrikidis, 2002),

$$G_{ij}(\boldsymbol{x} - \boldsymbol{x}_0) = -\delta_{ij} \ln(r) + \frac{\hat{x}_i \hat{x}_j}{r^2}$$

where $\hat{\boldsymbol{x}} = \boldsymbol{x} - \boldsymbol{x}_0$ and $r = |\hat{\boldsymbol{x}}|$

With above interpolations, $v = N_i \dot{\boldsymbol{P}}_i$ and $\sigma = \varphi_k F_k$

$$\begin{aligned} \int_\Gamma N_i \dot{\boldsymbol{P}}_i \varphi_j &= -\int_\Gamma \varphi_j \frac{1}{8\pi\mu_b} \int_\Gamma G F_k \varphi_k \, dS \\ \dot{\boldsymbol{P}}_i \int_\Gamma N_i \varphi_j \, dS &= -\int_\Gamma \varphi_j \frac{1}{8\pi\mu_b} \int_\Gamma G F_k \varphi_k \, dS \\ \dot{\boldsymbol{P}}_i M_{ij} &= A_{ik} F_k \end{aligned}$$

Using the results from the previous section

$$\begin{aligned} M^T \dot{\boldsymbol{P}}_i &= AF \\ A^{-1} M^T \dot{\boldsymbol{P}}_i &= F \end{aligned}$$

Multiplying both sides by M

$$M A^{-1} M^T \dot{\boldsymbol{P}}_i = MF = f$$

So finally we indentify the bulk Stokes damping matrix as,

$$D_{st} = M A^{-1} M^T$$

Numerical Integration

The difficult task is the evaluation of the matrix A. This is evaluated using numerical integration. This integration is complicate because of the existing singularity in the stokeslet function when $(\boldsymbol{x} = \boldsymbol{x}_0)$. To over come this problem different order of quadrature rules were used. Fig. 3.6. Eventhough theoratically different discritizations can be used for the membrane and the stokes formulations, in the actual implementation for same order b-splines were used.

$$A_{jk} = -\int_{u=0}^{u=1} N_j \left(\frac{1}{8\pi\mu_b} \int_{u=0}^{u=1} G N_k dS \right) dS$$

So the inner integration is done using one quadrature rule and the outer is done using another quadrature rule. Two rules can not have overlapping points if this happens the integration becomes a singularity. Like in the membrane dissipation the b-splines

change there definition at each knot point. Therefore,

$$A_{jk} = -2\pi \sum_{i=1}^{i=m-2p} \int_{u=u_i}^{u=u_{i+1}} N_j \left(\frac{1}{4\mu_b} \sum_{i=1}^{i=m-2p} \int_{u=u_i}^{u=u_{i+1}} GN_k a r du \right) a r du$$

Now we can use the numerical integration as

$$A_{jk} = -2\pi \sum_{i=1}^{i=m-2p} \left(\frac{u_{i+1} - u_i}{2} \right) \sum_{gj=1}^{N_{gj}} w_j N_j(u_{gj}) \left[\frac{1}{4\mu_b} \sum_{i=1}^{i=m-2p} \left(\frac{u_{i+1} - u_i}{2} \right) \sum_{gk=1}^{N_{gk}} w_k G(u_{gk}) N_k(u_{gk}) a(u_{gk}) r(u_{gk}) \right] a(u_{gj}) r(u_{gj})$$

N_{gj}, N_{gk} are respectively the outer and the inner Number of gauss points in side ith interval. w_j, w_k are the respective gauss weights in each gauss points. When both inner and outer integration happens in the same interval the singularity needs to be approximated. This was done using approximation for the elliptic integral of first kind. (Heltai, 2009)

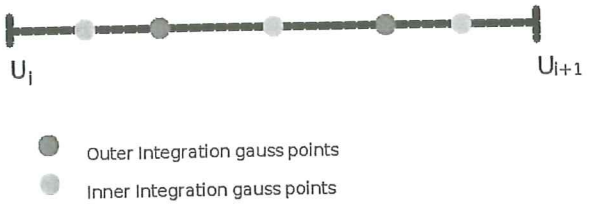

Figure 3.6: Different gauss rules for inner and outer integration

3.3 Explicit coupled solution method

With the b-spline discritization after calculating the damping matrix, constraint matrix and the energetic contribution we can assemble a simple time dependant equation

as

$$\begin{aligned} \boldsymbol{D}(\boldsymbol{P})\dot{\boldsymbol{P}} + \boldsymbol{L}(\boldsymbol{P})\boldsymbol{\lambda} &= \boldsymbol{f}_{elastic}(\boldsymbol{P}) \\ \boldsymbol{L}(\boldsymbol{P})^T\dot{\boldsymbol{P}} &= \boldsymbol{0} \end{aligned}$$

The constraint matrix includes the volume, area, and symmetry constraints. The volume constraint is kept as a option to analyze volume constrained case and the volume not constrained case. It has to be noted that the area constrain will be changed from global area constraint for L_2 dissipation to local area constraint for surface flow dissipation. To take the effect of surrounding fluid we just add the Stokes Damping matrix to the Membrane Damping matrix. So the final system of ODEs to be solved are

$$\begin{aligned} \Big[\boldsymbol{D}(\boldsymbol{P}) + \boldsymbol{D}_{st}(\boldsymbol{P})\Big]\dot{\boldsymbol{P}} + \boldsymbol{L}(\boldsymbol{P})\boldsymbol{\lambda} &= \boldsymbol{f}_{elastic}(\boldsymbol{P}) \\ \boldsymbol{L}(\boldsymbol{P})^T\dot{\boldsymbol{P}} &= \boldsymbol{0} \end{aligned}$$

We will consider initially a simple explicit algorithm,

$$\begin{aligned} \boldsymbol{D}(\boldsymbol{P}^n)\frac{\boldsymbol{P}^{n+1} - \boldsymbol{P}^n}{\Delta t} + \boldsymbol{L}(\boldsymbol{P}^n)\boldsymbol{\lambda}^{n+1} &= \boldsymbol{f}_{elastic}(\boldsymbol{P}^n) \\ \boldsymbol{L}(\boldsymbol{P}^n)^T\frac{\boldsymbol{P}^{n+1} - \boldsymbol{P}^n}{\Delta t} &= \boldsymbol{0} \end{aligned}$$

In the implementation the time stepping was done using the GNU Scientific Library(GSL). All the time stepping functions in that library can be used to do the time advance. All these time integrators have the capability of adaptive time stepping. It was set as a option to change from adaptive time stepping to constant time stepping.(software foundation GSL team, 2008) Discritisization, numerical integration and the solving was done using the subroutines available in A Finite Element Differential Equations Analysis Library(deal.II)(deal II team, 2009). To calculate the b-spline functions available (GSL) b-spline subroutines were used.

Embedded Runge-Kutta (2, 3) method.
4th order (classical) Runge-Kutta.
Embedded Runge-Kutta-Fehlberg (4, 5) method.
Embedded Runge-Kutta Cash-Karp (4, 5) method.
Embedded Runge-Kutta Prince-Dormand (8,9) method.
Implicit 2nd order Runge-Kutta at Gaussian points.
Implicit 4th order Runge-Kutta at Gaussian points.
M=1 implicit Gear method.
M=2 implicit Gear method.

Box 3.2: Available time integration schemes (software foundation GSL team, 2008)

Chapter 4

Relaxation dynamics of fluid membranes

Here the relaxation dynamics of the out of equilibrium membrane are analyzed. The shapes were generated by the static simulation by redusing the volume and/or the spontaneous curvature of the membrane. Then suddenly the spontaneous curvature was set to zero, or the volume constraint was released. The analysis are carried out with L2 dissipation, membrane dissipation, stokes dissipation and combination of membrane dissipation and stokes dissipation. The combined analysis of membrane and stokes flow is the one that physically more meaning full. So the main focus is on this will be on the coupled system.

4.1 Relaxation dynamics of fluid membranes

The numerical simulations were done for several shapes with volume constraint, and without volume constraint. For all the simulations the material properties were taken as,

4.1.1 Evolution in time without the volume constraint

The membrane is allowed to evolve in time by removing the volume constraint. In this situation only initial shape will finally evolve to a sphere, the basic shape with

Table 4.1: Material parameters used in the simulations

Parameter	Value
Viscosity of bulk fluid	$\mu_b = 1 \times 10^{-3}$ Nsm^{-2}
Viscosity of the membrane	$\mu = 5 \times 10^{-9}$ Nsm^{-1}
Bending rigidity of the membrane	$\kappa = 1 \times 10^{-19}$ J

minimum curvature energy. But the path of the time evolution is different from shape to shape. For the same initial shape and with initial conditions the time evolution followed by L2 dissipation and by the membrane dissipation is totally different. Here the Stokes dissipation can not be considered because physically bulk fluid will tend to constrain the volume. So considering Stokes dissipation without volume constran is not physically meaningfull. We analyzed three different shapes an Oblate Fig. 4.1, a Pearling Fig. 4.2 and a Stomatocyte. Fig. 4.3 (initial shape is in red)

In the figures some intermediate shapes were shown. They were not in constant time intervals. All the systems show very fast change in shape at beginning and then it goes down as it get close to the shape of the circle. Surface area is conserved up to order of magnitude 10^{-4}. The time integrate used have some affect on the surface constraint. If the time integration is a very stable one then it can be seen that the surface area is more conserved. The simulation results for the time evolution for these three shapes were shown in Fig. ??. The graphs clearly shows that the membrane dissipation and L2 dissipation time evolution is altogether different. It has to be noted that the time was scaled down to fit in the same range. The stomatocyte and the pearling are discontinuously transformed shapes from oblate and prolate. But the relaxation paths with the volume constraint removed do not resemble any connection between them. In the log log scale graphs of the dissipation one can see a disscontinuity in the Oblate in the membrane dissipation, but this disscontinuity is compleatley dissapiered in the L2 dissipation. Fig. ??. Here it is appeared as a change in the continuity of the energy.

For the oblate the L2 dissipation is higher than the membrane dissipation and for

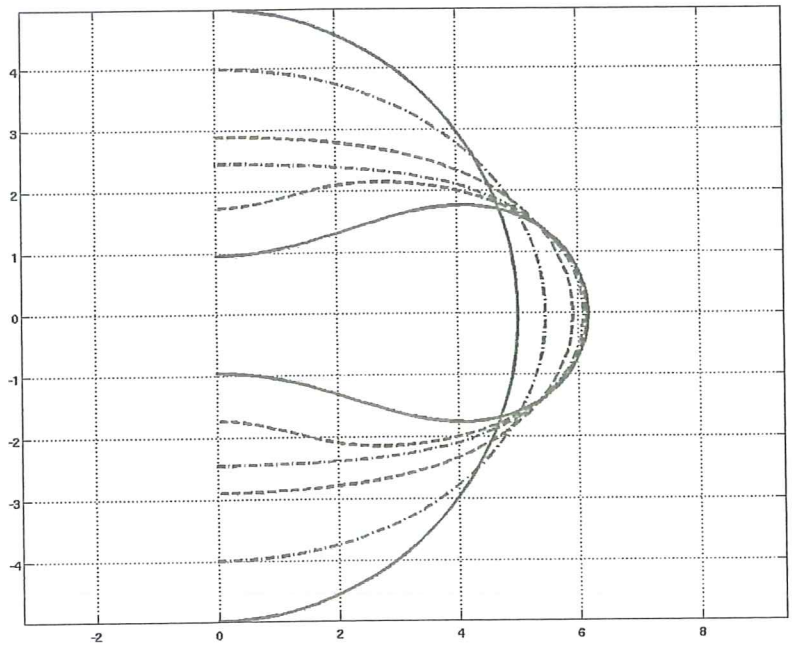

Figure 4.1: Time evolution witout volume constraint - Oblate

pearling and stomatocyte shows the opposite behavior, in general it is not possible to come to a conclusion that wether L2 or membrane dissipation is higher, this will entirely dipend on the shape being analyzed. Time evolution of the energy is very consistant and invariant of reparametrization in most of the time. There can be miniature fluctuation but these will disapier when the integration quadrature increased or when a small time step is used. The time advancement of the dissipation is not so consistant or invariant with reparametrization. There can be spike coming out corresponding to each reparametrization. The time evolution of the three shapes without volume constraint is shown in Fig. 4.4, 4.5, 4.6. This clearly shows the different paths taken by the shapes.

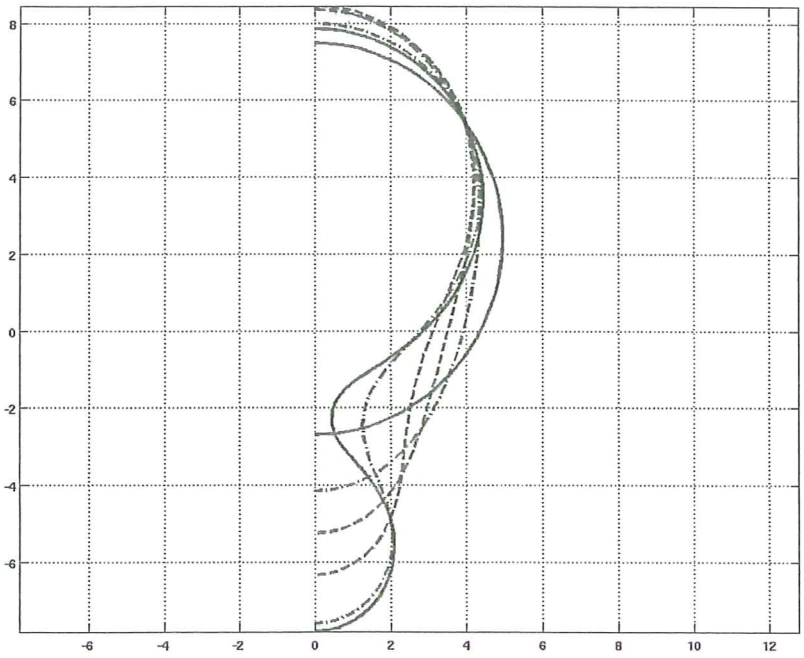

Figure 4.2: Time evolution witout volume constraint - Pearling

4.1.2 Evolution with volume constraint

The relaxation with both surface constraint and volume is considered here. This can be understand as setting the spontaneous curvature C_0) to zero. With the volume constrained only the discontinuously transformed shapes such as stomatocyte, pearling, will undergo relaxation. Shapes like oblate or prolate do not undergo relaxation with volume constrained because theory are in the equilibrium state and we are not changing anything in there environment. Numerical simulations were done with stomatocyte and pearling.

The relaxation dynamics of the membrane under L2 dissipation, membrane dissipation and stokes dissipation is shown in the Fig. 4.9. The time difference in L2 dissipation and membrane dissipation can be clearly seen for both pearling and for stomatocyte. Membrane dissipation and stokes dissipation takes same order of time

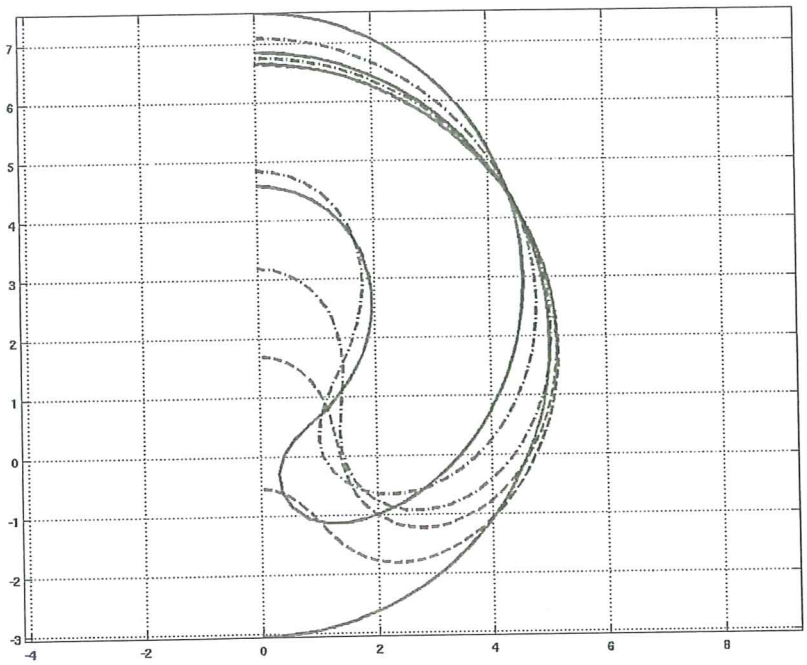

Figure 4.3: Time evolution witout volume constraint - stomatocyte

to relax. It can be seen that for pearling the membrane dissipation is faster than stokes flow but for the stomatocyte stokes dissipation is faster. The simulation for the stomatocyte with membrane dissipation is not completed, maybe because of numerical instabilities. When the energy is plotted in log scale the difference paths follow by the two shapes clearly visible. Pearling undergoes very gradual transformation, but the stomatocyte at the beginning very slow and then it change the shape drastically in a very short time. It is not possible to do a complete simulation of the stomatocyte with only membrane dissipation passing this very fast shape change, all the simulations stuck in this region. The simulations with only stokes flow or with both stokes and membrane disspation was done upto the final equilibrium state. In the log scale it can be seen that all the three dissipations follow similar shaped paths when the volume is constrained. They show differences in relaxation time but gen-

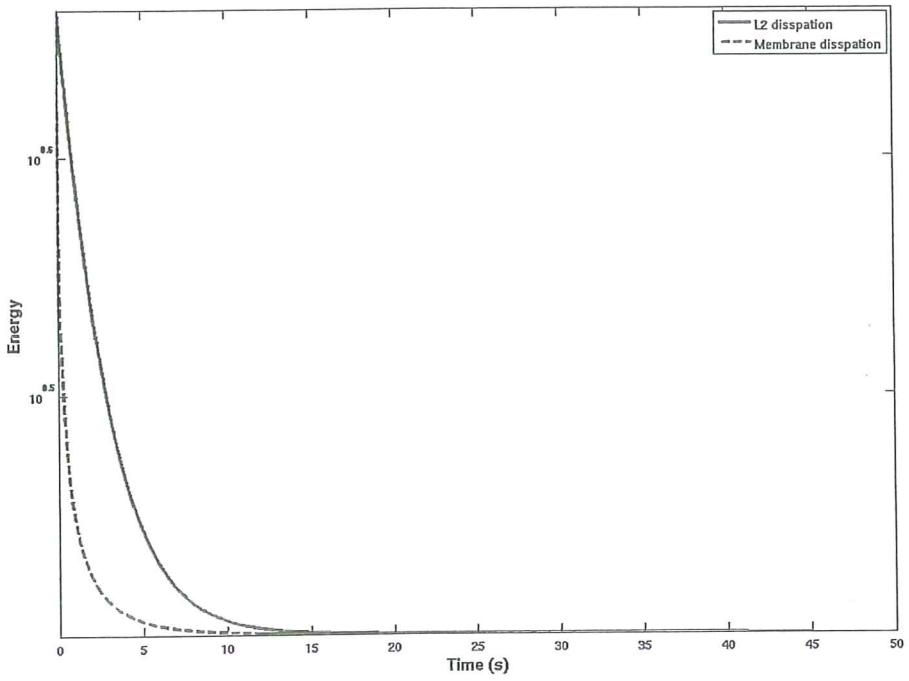

(a) Energy

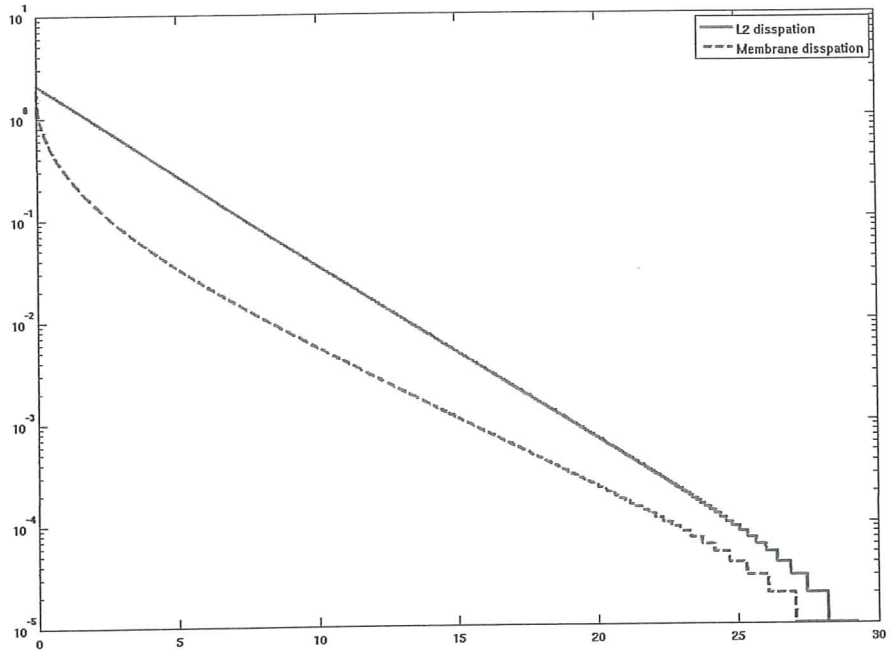

(b) Energy semi-log

Figure 4.4: Oblate

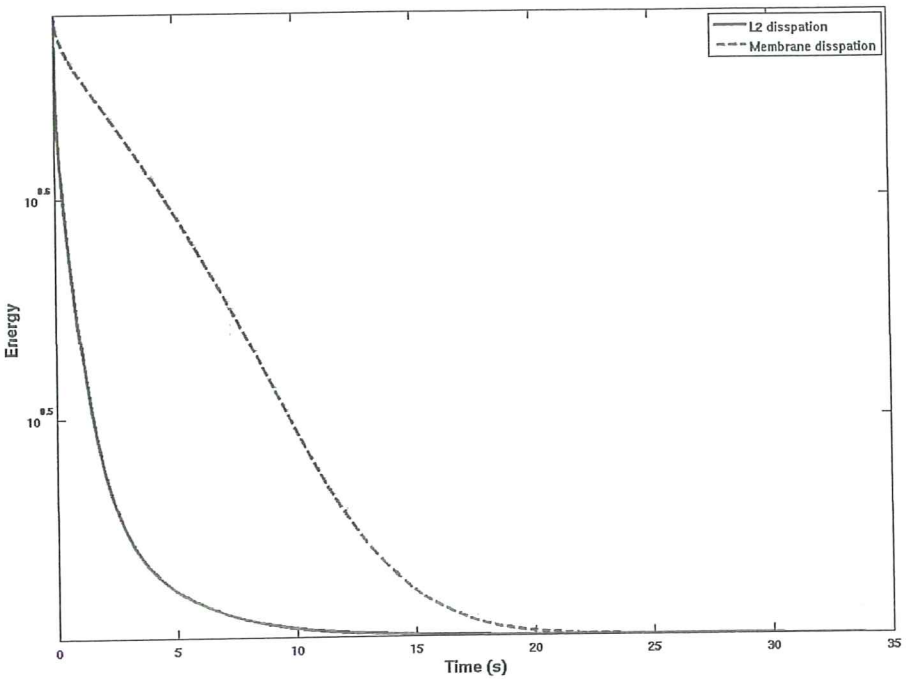

(a) Energy

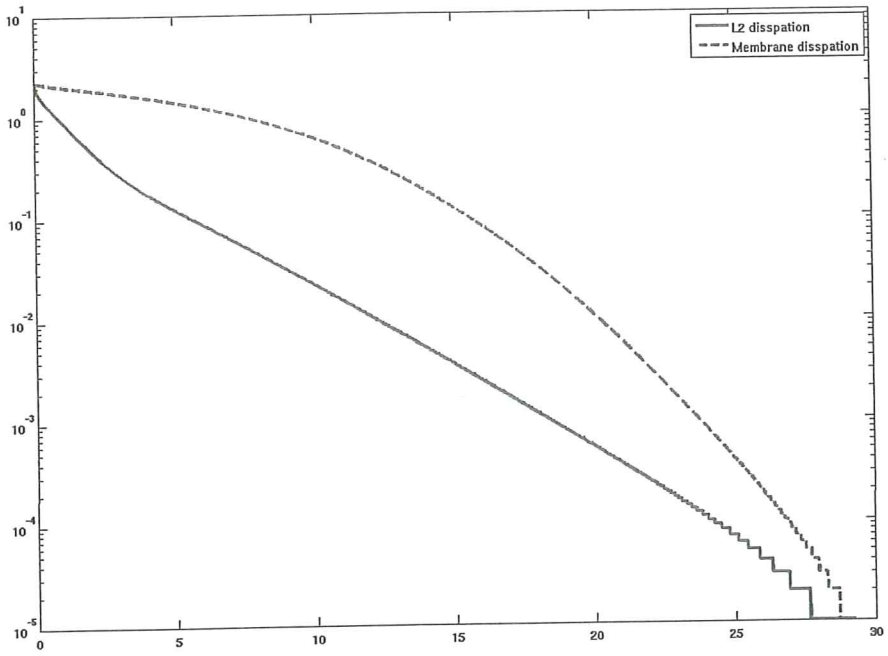

(b) Energy semi-log

Figure 4.5: Pearling

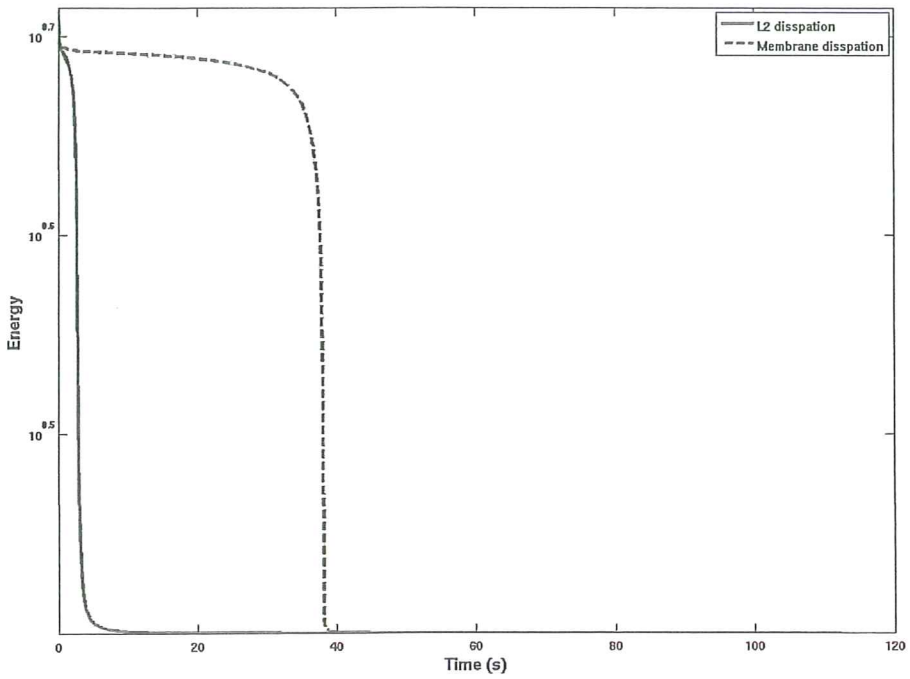

(a) Energy

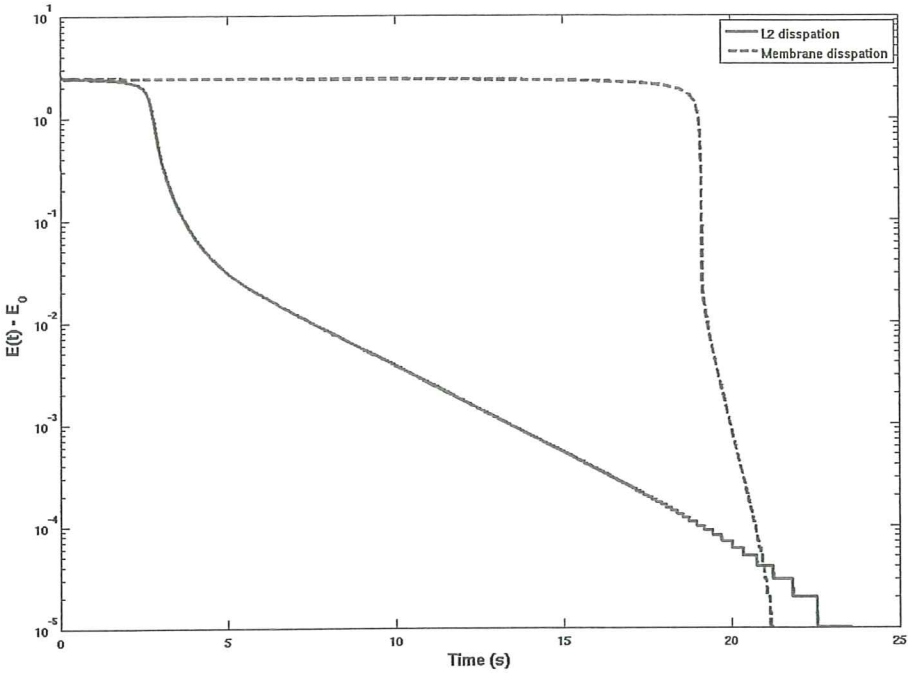

(b) Energy semi-log

Figure 4.6: Stomatocyte

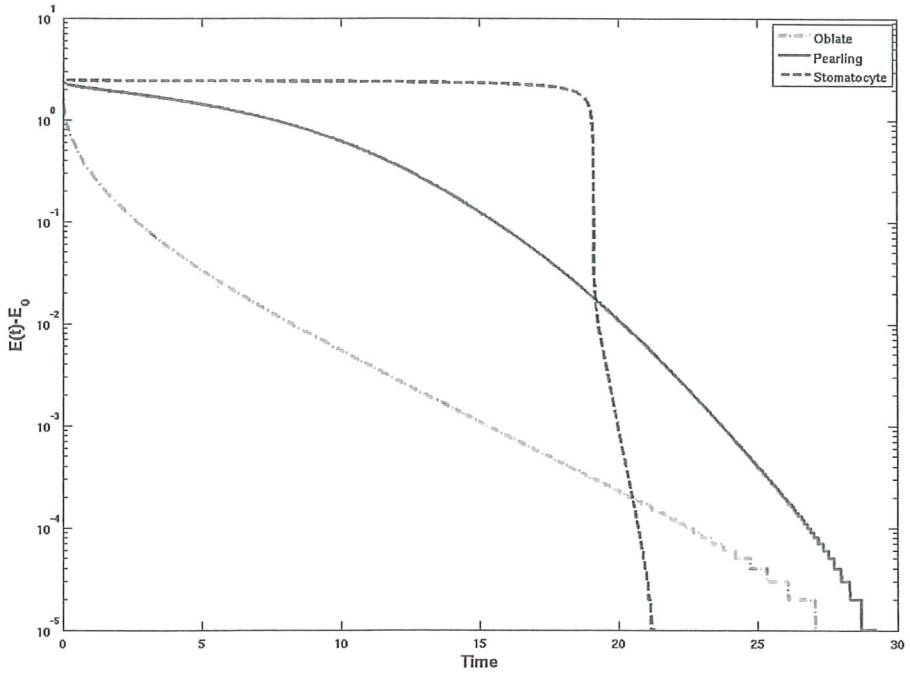

Figure 4.7: Time evolution of different shapes with membrane dissipation

erally graphs shows similar behavior. Dissipation rate for pearling follows a gradual and steady change in the simulations, but the simulations for stomatocyte shows lots of spikes in the dissipation at each reparametrization. If the dissipation for the stomatocyte is closely examined one can see the increase in the dissipation rate in its rapid transformation stage. This stage is almost a vertical straight line in log scale plot. The relaxation was assumed to be acting like a spring damper system if this is true it should show an exponential decay. The graph of $\log(E - E_0)$ and the time should be a straight line because

$$E = e^{\alpha t + c} + E_0$$

Here E_0 is the energy of the equilibrium shape and α, c are constants. Fig. 4.10 shows this clearly, both pearling and the stomatocyte shows a linear decay in semi

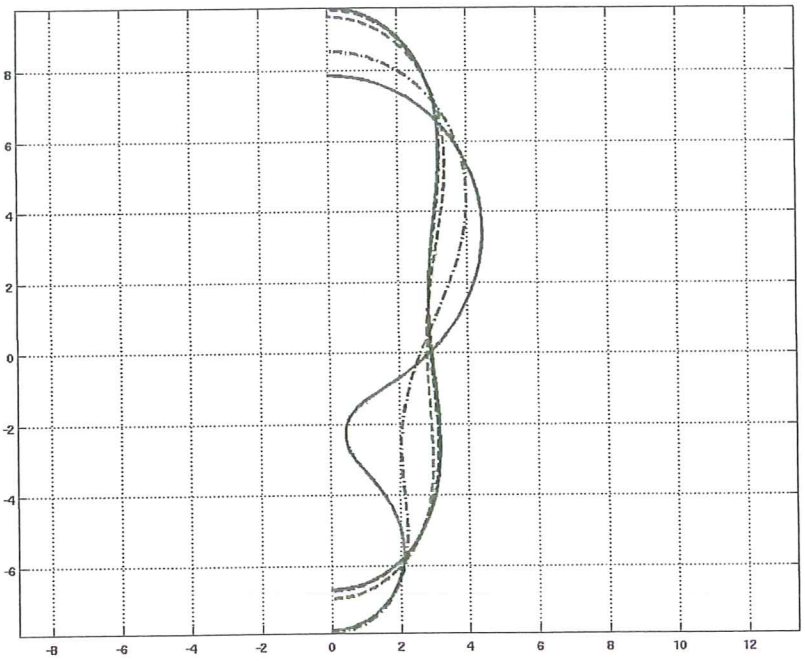

(a) Pearling

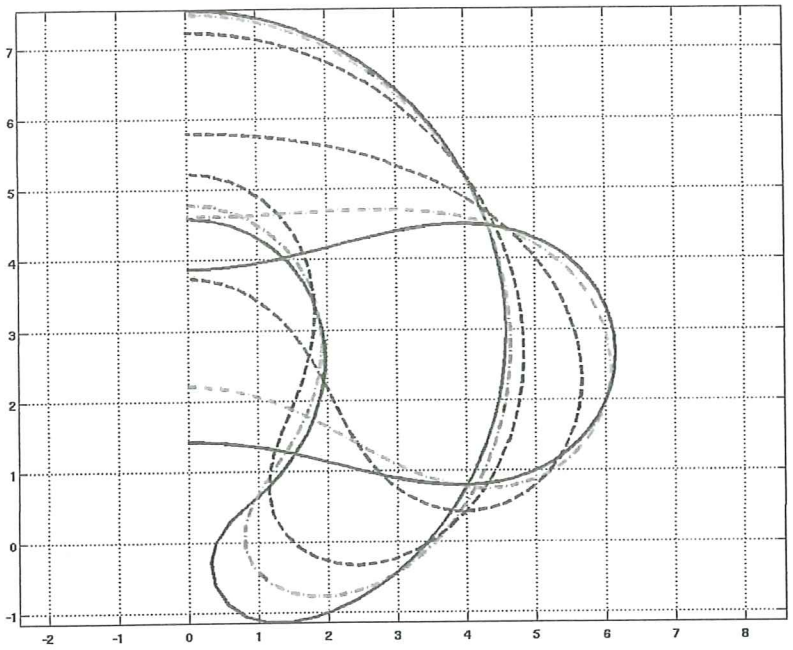

(b) Stomatocyte

Figure 4.8: Time Evolution with volume constraint

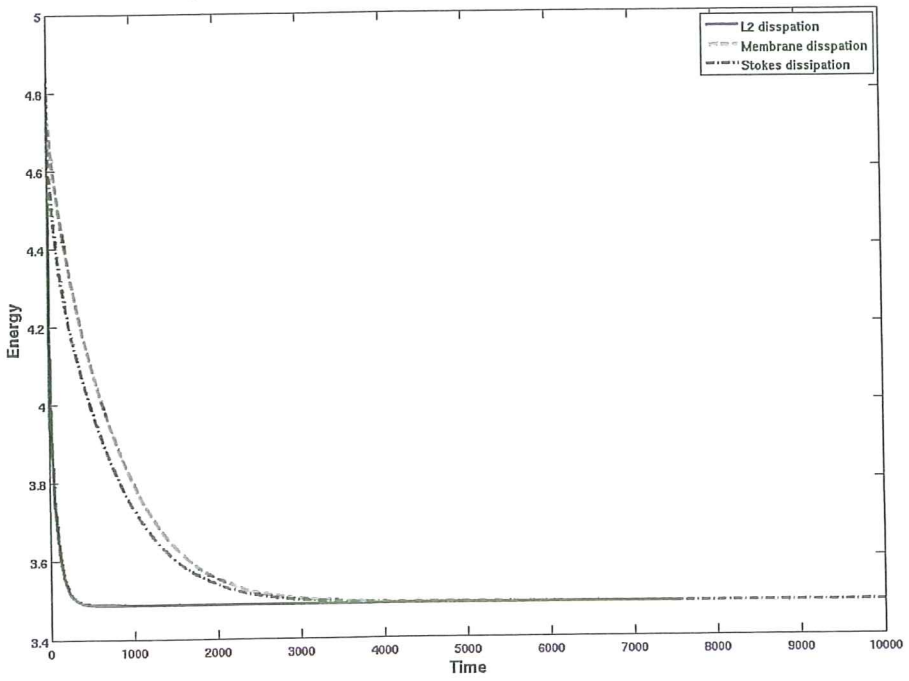

(a) Pearling

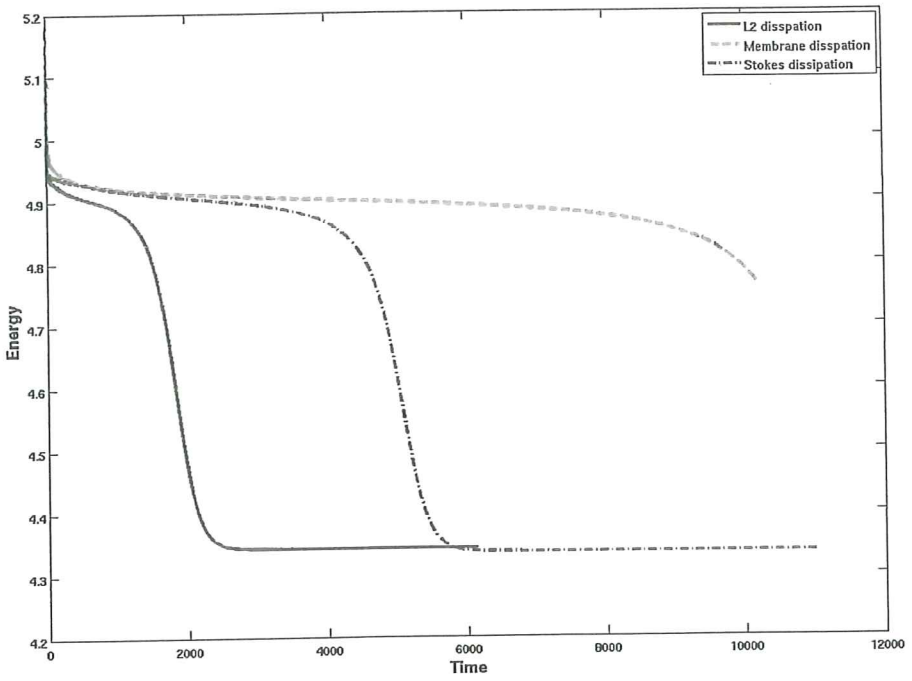

(b) Stomatocyte

Figure 4.9: Energy - with volume constraint

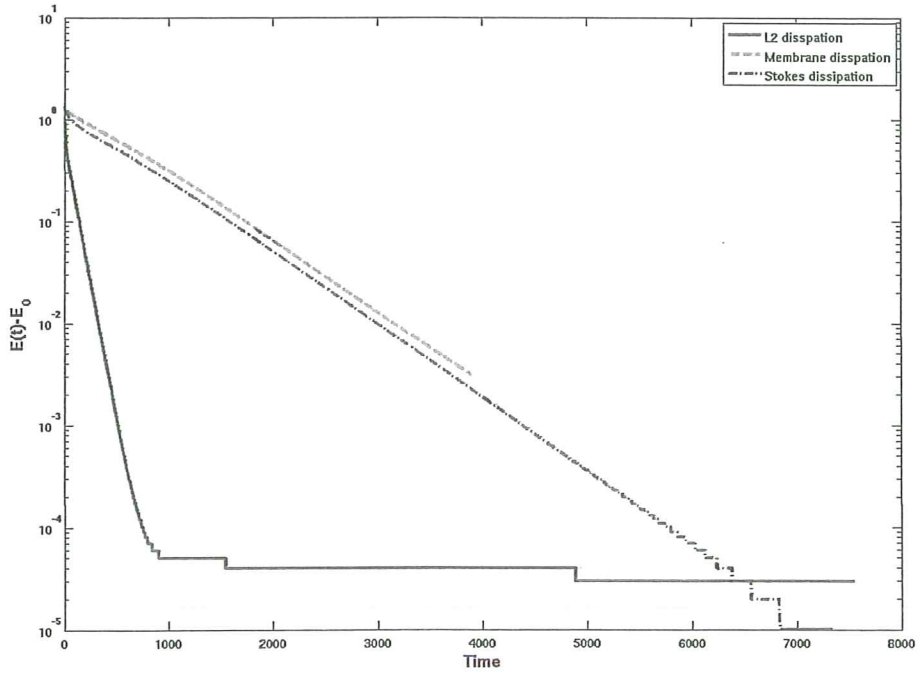

(a) Pearling

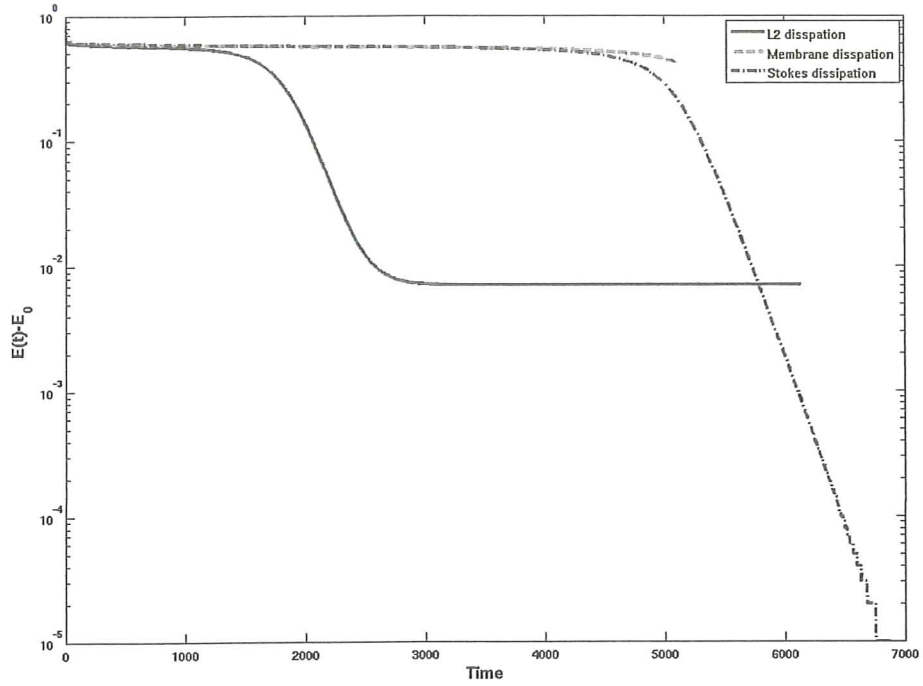

(b) Stomatocyte

Figure 4.10: Exponential behavior

log scale. In this plots it can be seen that stokes flow and the membrane flow both follow behavior but with different α values (see the difference in slope for stokes dissipation and for membrane dissipation). It is interesting to note that the behavior of the stomatocyte, in this semi log scale at the beginning it is almost a horizontal straight line and then it shows the exponential decay corresponding to the rapid shape changing region.

4.1.3 Characteristic length

With the material parameters used in the simulations the characteristic length $l_2 = \frac{\mu}{\mu_b}$ (Arroyo and DeSimone, 2009) will be 5 μm. Above this length scale bulk viscosity is the dominant dissipative mechanisum where below, membrane viscosity dominates. If the vesical is larger than this length the relaxation time is given as $\frac{\mu_b R_0^3}{\kappa}$ and if the vesical is smaller than this length relaxation time is given as $\frac{\mu_b R_0^2}{2\kappa}$ (Arroyo and DeSimone, 2009). Here R_0 is the radius of the generating sphere corresponding to that shape. Several simulations were carried out for the same shape with changing R_0. The Fig. 4.11 shows the results in log log scale for pearling, the change of the slope can be identified exactly at the length of $l_2 = 5\mu m$. Radius smaller than this (red colour) and radius lager than this (blue colour) almost follow a straight line showing this behavior.

This suggests a new method to measure the membrane viscosity, by recording experimentally the cahnging size $R_0 = \frac{\mu}{\mu_b}$. This parameter is otherwise very difficult to measure.

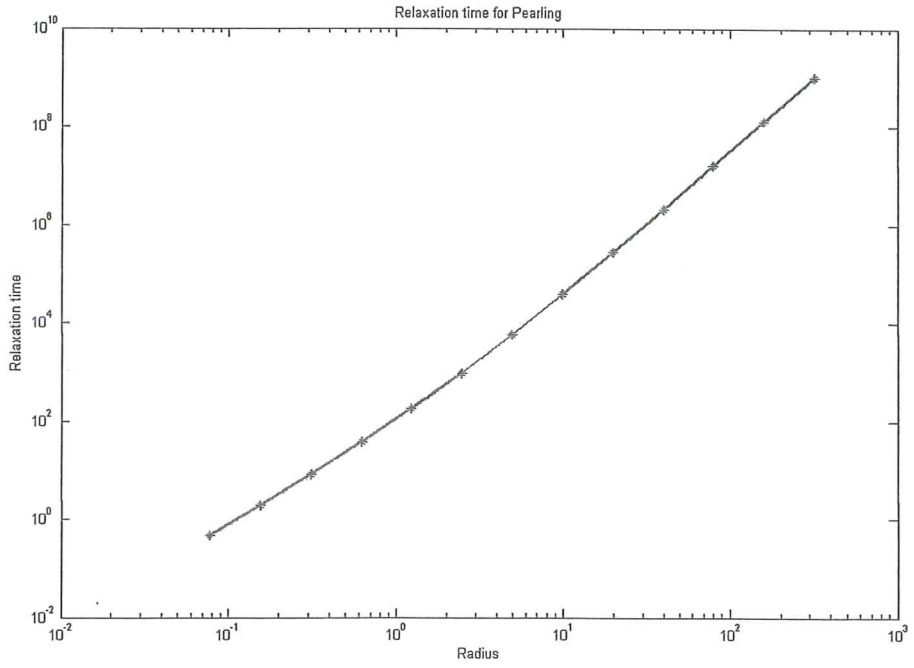

Figure 4.11: Relaxation time

Chapter 5

Conclusions

This project models the dynamics of fluid membranes, with an emphasis on the effect of the membrane flow dissipation coupled with the stokes dissipation due to surrounding fluid. Unlike the L_2 gradient flow, the membrane flow considers the lateral motion within the membrane surface of the fluid particles making up the membrane. The first two chapters disscuss about some biological aspects of the problem, the hypothesis taken and explain the numerical modeling and implementation chosen. Third chapter gives a detailed explanation about how the discretization was done and details about the numerical implementation of the system. In this chapter a brief introduction about the b-splines and the boundary element methods were also included. The fourth chapter focused on the results obtained from the simulations. In this chapter we were able to predict the expected behavior of the system.

This study is only the beginning of the relaxation dynamics of biological membranes coupled with the Stokes flow. The whole study was done assuming that system has only the membrane and the surrounding fluid so that membrane do not have any effect of other similar membranes directly in touch with it and the boundary for the sourrounding fluid is the infinity. In reality this is not true, the membranes are not along in a real situation, they can be enclosed inside another membrane like the internal organalles of a cell or there can be lot of other membranes which are located very close to each other like in a colony of bacteria or the sourrounding cells. They may be touching each other giving rise to coupled problems with two membranes and the Stokes flow with enclosed boundary and on the effect of the sourrounding objects.

Even for this very simple case there are lot to be done about the numerical stability of the system, still it is not possible to simulate all the shapes generated from the static code. Boundary element method needs to be improved. Currently it has an integration error due to the singularity of the kernel at the corner elements which gets higher and higher with the number of elements increased (Heltai, 2009).

On the other hand, this project only models vesicles of one component. The line tension between two different components which induced budding can be modeled to have a more realistic model. To represent the entire budding, the last thing to add, is the separation of one vesicle in two. This kind of study was done before and leads to a lot of different and interesting shapes but this study is not realistic biologically. These are some ideas which would allow us to go deeper into in the subject but there are many more ways of study:non-asymmetric shapes, topologically variant shapes, others energetic mechanisms and interactions.

Bibliography

Arroyo, M. and A. DeSimone (2009). Relaxation dynamics of fluid membranes. *Physical Review Letters 79*.

Blood, P. D. and G. A. Voth (2006). The Cauchy relations in a molecular theory of elasticity. *Proceedings of the National Academy of Sciences 103*(41), 15068–15072.

deal II team (2009). deal ii library documentation. `http://www.dealii.org/6.2.0/doxygen/deal.II/index.html/`.

E.Lindahl and O.Edholm (2000). Mesoscopic undulations and thickness fluctuations in lipid bilayers from molecular dynamics simulations. *Biophysics journal 79*, 426–433.

Gaba, E. (2006). Minimal surface curvature planes. `http://en.wikipedia.org/wiki/File:Minimal_surface_curvature_planes-en.svg`.

Grosjean, L. (2008). Numerical simulation of the dynamics of fluid membranes. Master's thesis, Universitat Politecnica de Catalunya, Departament de Matematica Aplicada III.

Heltai, L. (2009). Swimmers. internal reports SISSA.

Karlsson, M., K. Sott, M. Davidson, A. Cans, P. Linderholm, D. Chiu, and O. Orwar (2002). The Cauchy relations in a molecular theory of elasticity. *Proceedings of the National Academy of Sciences 8*(2), 169–186.

Laboratory, M. A. I. (2004). Bzier curve and b-spline curve. `http://groups.csail.mit.edu/graphics/classes/6.838/S98/meetings/m15/`.

Peegl, L. A. and W. Tiller (1997). *The NURBS book*. Springer Verlag.

Port, A. (2004). Structure of an animal cell. `http://www.animalport.com/animal-cells.html`.

Pozrikidis, C. (2002). *A Practical Guide to Boundary Element Methods*, Chapter Viscous flow. Chapman and Hall.

Ruiz, M. (2007). Cell membrane detailed diafram. http://en.wikipedia.org/wiki/Image:Cell_membrane_detailes_diagram.svg.

Seifert, U. and R. Lipowsky (1995). *Handbook of Biological Physics*, Volume 1, Chapter Morphology of Vesicles. Elsevier Science B.V.

software foundation GSL team, F. (2008). Gsl reference manual. http://www.gnu.org/software/gsl/manual/html_node/.